AD 277 523

Department of AERONAUTICS and ASTRONAUTICS
STANFORD UNIVERSITY

NOX

B. HEGGLIN

DYNAMIC BUCKLING OF COLUMNS

JUNE
1962

Technical Report No. 3
Prepared for the Office of Naval Research of the U.S. Navy
Under Contract Nonr-225(47)
Project NR 064-434

SUDAER
NO. 129

Department of Aeronautics & Astronautics
Stanford University
Stanford, California

DYNAMIC BUCKLING OF COLUMNS

by

Bruno Hegglin

SUDAER NO. 129

June 1962

The work here presented was supported by the
United States Navy under Contract NONR 225(47), monitored
by the Mechanics Branch of the Office of Naval Research.

ACKNOWLEDGMENT

The author wishes to express his sincere appreciation to Dr. Nicholas J. Hoff for his scientific guidance and to his supervisor Brian Lempriere for his advice and assistance in the conduct of this project.

He is grateful for the sponsorship of the United States Navy through Contract Nonr 225(47).

TABLE OF CONTENTS

TABLE OF CONTENTS (Cont'd)

NOTATION

A	total cross-sectional area
E	Young's modulus
F	total deflection of middle of column from straight line; $F = Y(L/2) + e\rho$
I	moment of inertia
L	length of column
N	rotational speed of flywheel in rpm
P	total axial force
P_{max}	max. total axial force attained during loading process
P_E	Euler load; $P_E = \pi^2 EA/(L/\rho)^2$
X	coordinate along axis of column
Y	total deflection at station X from initial position of column
a_s	velocity of sound
c	loading head velocity
e	eccentricity, initial deviation of middle of column from straight line as a fraction of ρ
f	non-dimensional form of F ; $f = F/\rho$
h	column thickness
s	slenderness ratio; $s = L/\rho$
t	time
t_{max}	time elapsed until P_{max} was attained during loading process

NOTATION (Cont'd)

Ω dynamic similarity number; $\Omega = \pi^8 (a_s/c)^2 (\rho/L)^6$

α load factor; $\alpha = P/P_E$

α_{max} maximum value of load factor attained during loading process; $\alpha_{max} = P_{max}/P_E$

ϵ strain in column

$\bar{\epsilon}$ average strain in column due to P

ϵ_b midpoint bending strain due to bending of column

ϵ_E Euler strain; $\epsilon_E = \pi^2/(L/\rho)^2$

δ displacement of upper column end

δ_{max} displacement of upper column end when P_{max} is attained during loading process

ρ radius of gyration; $\rho = h/\sqrt{3}$

σ stress in column

ϕ angle of flywheel covered by cam

ξ non-dimensional displacement of upper column end; $\xi = ct/L\epsilon_E$

ν rotational speed of flywheel in sec^{-1}; $\nu = N/60$

C, C_1, C_2, C_3, C_4, C_5, C_6, x, y, y_o as defined in the Appendix

INTRODUCTION

The purpose of this paper is to present experimental results of dynamic buckling tests of columns in which plastic deformation was expected to occur. To obtain a comparison with the tests carried out at the Polytechnic Institute of Brooklyn, the present tests were performed in the same range of the dynamic similarity number as those in Brooklyn; however the similarity numbers were obtained with shorter columns and higher loading velocities to accomodate shorter columns and to provide more rigidity and reliability. As a consequence many components of the mechanical part and nearly the whole electrical part of the machine have been redesigned and new methods in recording were used.

I. ALTERATIONS OF THE TEST MACHINE-MECHANICAL PART

When the machine was received from Brooklyn, it was in a bad working condition. It was first restored to its original state. A few tests however showed that higher requirements had to be met. Above all certain parts such as the plunger-spacer assembly and the synchronization mechanism had to be less susceptible to failure. It also turned out that there was a lack of rigidity of the parts carrying the lower knife edge. Another requirement was the increase of head velocity to about four times the head velocity used in previous tests. Furthermore a load transducer had to be built to allow load measurements when the yield limit of the columns was exceeded and strain gages on the column would not be applicable. Thus many components of the machine were gradually altered and redesigned before the test series were started.

1. PLUNGER-SPACER ASSEMBLY

The spacer has been only slightly changed in its dimensions. The connection to the solenoids by means of stiff wires screwed into the spacer turned out to be unreliable. Subsequently a steel strip was used which was fixed to the spacer by three rivets (see Fig. 1). The solenoid armatures occasionally locked because of their looseness when pulled out of the solenoids. A smooth motion was obtained later through an axle fixed to the armatures and passing through the stationary part of the core. At the same time a rubber stop was provided. In the later tests the system proved to be very reliable even when it was operating at the highest speeds.

The upper plunger was not changed. The lower plunger was changed first to accomodate the load transducer in order to save space. For this reason it had to be widened considerably. Unfortunately it turned out later that the location of the load transducer at the top of the column was disadvantageous as far as noise is concerned. It was moved to the lower end of the column and replaced by a rigid plunger of the same outside dimensions (see Fig. 3).

2. BOTTOM PIECE (Fig. 4), CLAMPING PLATES (Fig. 5)

Measurements showed that the main screw could never be used alone as a rigid support of the lower knife edge. In certain positions it was quite loose and could easily be moved laterally. For this reason a large, heavy bottom piece was provided. It was to fit accurately between the two vertical plates, its length being just a little less than their width so that it could be very rigidly clamped by two front plates. In this way the main screw served essentially only the purpose of raising and lowering the bottom piece and of taking over a small part of the load. The transducer unit was then mounted in the bottom piece by a press fit. It should be mentioned that despite the rigidness and the heaviness of the bottom piece a slight movement could be noted later as a function of the load. Because of the bottom piece the machine could not accomodate columns in excess of 8 3/4 in. length.

3. END PIECES (Fig. 2)

The end pieces were made as small as possible in order to reduce inertial effects. Relatively large screws with fine pitch (1/4" - 28) allowed rigid clamping on the columns and accurate setting of the eccentricity. The inside was ground for proper contact with the columns. The outside grooves (counterparts of the knife edges) were ground also after the whole piece had been hardened. Special attention was given to the inner radii as they turned out to be critical locations as far as cracks are concerned.

4. LOAD TRANSDUCER UNIT (Fig. 6)

A load transducer built in the test machine became necessary when tests involving plastic deformation of the columns were planned. The load transducer unit subsequently designed consists essentially of an outer housing which in turn consists of two parts sliding in each other and an inside short length of steel tubing provided with two strain gages. Special provisions were made for the arrangement of the leads. As a small preload is necessary to keep the column in place before the test, a helical spring was built in such a way that the preload did not

exceed 6 lbs. Two strain gages mounted apart from the load transducer unit were used as dummy gages.

A very important requirement for the transducer was that its deformation relative to the deformation of the column should be small, say smaller than 5%. Calculation of the deformations showed that the tube shortened by 1.95% of the shortening of a straight column 8.5 in. long; with other columns the corresponding values were: 2.26% with a 7.5 in. column, 2.61% with a 6.5 in. column and 3.08% with a 5.5 in. column. All these values are well within the margin of the requirements especially since lateral deflection of the column was ignored. This type of load transducer turned out to be sensitive enough if used with high amplifier gain, and at the same time it was very reliable. Load transducers of the inductive type were investigated earlier and were found to be less suitable.

5. DEFLECTION CANTILEVER (Fig. 7)

To determine the head velocity, the displacement of the column head had to be measured. A cantilever of the type used in earlier tests at Brooklyn Polytechnic Institute seemed to be most promising. The increased head velocity however caused some difficulties with a long cantilever as bending vibrations were generated. Subsequently a new cantilever was designed consisting of a rather stiff stainless steel plate three and one-half inches long. It was preloaded so that proper following of the knife edge on the lower plunger was insured. Strain gages were attached as close to the root as possible. The whole unit was then screwed rigidly on the sides of the two vertical plates of the machine. In addition the U-piece holding the cantilever beam was clamped by wedges against the vertical plates to eliminate all vibrations of that part.

II. ALTERATIONS OF THE TEST MACHINE-ELECTRICAL PART

1. SYNCHRONIZATION MECHANISM (Fig. 8)

The synchronization mechanism represented the most difficult part in the redesign of the test machine as the head velocity in our tests was increased by roughly a factor of four over that of previous tests. A typical test of the new program was of 4.5 msec duration and thus the flywheel had to make one revolution in 27 msec. Hence there were 22.5 msec left for the mechanism to actuate the spacer in or out, respectively. The following actions had to be controlled by the synchronization mechanism:

(a) pull the spacer in as soon as possible after the cam has passed the lower plunger;

(b) keep the spacer in the engaged position until the loading process has been completed; then

(c) pull the spacer back so that no further loading and hammering of the column can take place.

As the whole process could be divided into four time periods, a contact wheel was designed consisting essentially of an insulating material with a quarter sector of metal rotating at a quarter speed of the flywheel. Four contact brushes were provided around the periphery of the wheel at various intervals. A fifth contact brush served the oscilloscope triggering system.

The sequence of events in the loading process then was as follows:

(a) in the first time period the circuitry had to be closed after the operator pushed the load-button. This could happen at any time during a revolution of the flywheel;

(b) the second time period started at the moment when the flywheel cam passed the lower plunger. Then the IN solenoid was energized so that it pulled the spacer between the upper and lower plungers. On the next sweep of the cam a uniform displacement with respect to time was imposed on the column head by the cam. The spacer was kept in the engaged position until the loading process was completed.

(c) the third time period began immediately after the flywheel cam passed the lower plunger, the OUT solenoid was energized and the spacer was retracted.

(d) at the beginning of the fourth time period the circuitry was opened so that no further action could take place. The circuitry would not close again unless the operator pushed a special ready-button.

In order to reduce electronic noise in the recording equipment the voltage of the synchronization mechanism had to be kept as low as possible; on the other hand high operating speed required high voltage for the solenoids. Therefore a step transformer was inserted which had output voltages from 100v up to 200v in steps of 20v allowing an optimal setting. Several condensers were provided in order to reduce electronic noise.

A full explanation of the functioning of the synchronization mechanism is too tedious to be given here. However, the functioning of the mechanism can be understood from the circuitry diagram of Fig. 8.

2. INSTRUMENTATION FOR RECORDING THE DATA (Fig. 9)

Preliminary test records were made using a CEC Recording Oscillograph (Galvanometer type). A problem arose in that the chart speed could not be increased sufficiently. Other considerations such as time and cost of such chart recording led to the choice of a dual-beam DuMont Oscilloscope with built-in trigger together with a Fairchild Polaroid Camera.

In the preliminary test series load and column head displacement were recorded. Later as the speed of the machine and thus the column head velocity was theoretically kept constant at a known value one trace was used for the column midpoint bending strain and the other for the load recording. In each case the signals came from strain gage bridges supplied by 10 volts DC from car batteries. They were fed into a Sanborn Preamplifier, Sanborn Amplifier and from there into the oscilloscope. All the leads were shielded to prevent them from picking up electronic noise which had been a serious problem for a long time. In order to have a time signal on the records a simple sine wave from a signal generator

was fed into the oscilloscope and recorded immediately before each test on the same picture that was used afterwards for the test records. The frequency was carefully set against the line frequency by forming Lissajous figures. Of course, once the time signal was recorded the sweep vernier had to be kept fixed.

In order to get only one sweep of the two beams over the screen at a predetermined time, a triggering system had to be designed. The two traces could be released by shorting the trigger input of the oscilloscope to ground. The ground signal was obtained over the fifth brush at the contact wheel which was only possible when the circuitry of the synchronization mechanism was closed.

III. EQUIPMENT FOR SETTING AND MEASURING SYMMETRY AND ECCENTRICITY OF COLUMNS

1. COLUMN STRAIN GAGE CIRCUITRY

On the wider sides of each column three strain gages, two at the sixth points and one at the midpoint were provided. Strain gages of the type BLH SR - 4 and Shinkoh Type S_{11} were used. Inserted in various ways into the circuitry they served a triple purpose:

(a) to check the symmetry

(b) to measure the average strain in order to determine the applied load; and

(c) to measure the midpoint bending strain.

For the strain gage circuitry to serve the triple purpose a special switch box shown in Fig. 11a had to be designed with controls having three positions. To facilitate the understanding of Fig. 11a the circuitry has been redrawn in Fig. 11b in a simplified form for each of the three connections.

2. INSTRUMENTATION

Nearly all the checks and measurements were made with a BLH SR - 4 Type N Strain Indicator, which was adequately sensitive and which replaced an older system built of a strain gage power supply, an amplifier, a Wheatstone - bridge and some reading instrument.

IV. TESTING OF COLUMNS

1. PREPARATION OF THE COLUMNS; MATERIAL CONSTANTS

All the columns were carefully machined in a milling machine as follows: for the preliminary test series only the ends, and for the main test series the wider sides also. Smooth ends were necessary in order to have proper contact between the column and the end pieces. Moreover, the experiments showed that results from columns machined on the wider sides were more consistent than those obtained with columns that were not machined in this manner.

The material of the columns was an extruded aluminum alloy with the designation ALCOA 2024 - T4. The following data are taken from "Metals Handbook", 8th edition:

Ultimate strength	68,000 lb/in.^{2}
Yield strength	47,000 lb/in.^{2}
Modulus of elasticity	10.6×10^6 lb/in.^{2}
Poisson's ratio	0.33
Velocity of sound	199×10^3 in./sec

2. SETTING AND MEASURING SYMMETRY AND ECCENTRICITY

The procedure of setting the columns was as follows: The end pieces were first rigidly screwed onto the columns under a light load so that no gap between column and end pieces was possible. All subsequent adjustments and measurements were made in the test machine. First it was insured that with the circuitry set for symmetry check the reading of the strain indicator was zero, when this was accomplished it was said that the column was symmetric. The symmetry check had to be repeated after each screw adjustment. By means of a Southwell plot the eccentricity could be determined and adjusted. The Southwell plot was based on the readings obtained when the circuitry was set for measuring load and midpoint bending strain, respectively. These procedures were extremely tedious, the more so the smaller the eccentricity was. Nevertheless they had to be carried out as accurately as possible because of the importance of the eccentricity. The columns were left in the machine until the test was over so as not to disturb the final setting.

3. GENERAL TEST PROCEDURE

After the column had been adjusted for symmetry and its final eccentricity measured, it was kept in place by a small load of approximately 6 lbs exerted by the transducer spring until the actual test took place. All the electronic instrumentation had been switched on at least half an hour before so that there would be no drift. The bottom piece was raised as high as possible without exceeding the spring load of the transducer. It was then very rigidly clamped in that position. Subsequently the time signal was recorded, all the leads connected for the actual test and the instrumentation and machine checked and serviced thoroughly. This included among other things checking spacer position, lubrication of plunger-spacer assembly, cleaning contact wheel and greasing the flywheel cam. The voltage of the battery supplies for the various strain gage circuits was checked right before and right after each test and when necessary adjusted by a potentiometer. Finally the motor was started; when full speed was attained the operator threw a ready-button, opened the shutter of the camera, pressed down the load-button and the actual test took place. Subsequently the shutter of the camera was closed, the power for the electric motor interrupted and the machine stopped by a built-in automobile brake.

4. CALIBRATION OF THE LOAD TRANSDUCER, THE DEFLECTION CANTILEVER AND MIDPOINT BENDING STRAIN

Calibrations for the load transducer were made before the preliminary tests and both before and after the two main Test Series using a universal hydraulic test machine and all the standard equipment used later for the dynamic tests. Two calibration curves are shown in Fig. 12 for two amplifier attenuator settings.

The calibration of the deflection cantilever was made first in a special jig carrying the cantilever unit and allowing easy access for the measurements. Later the necessary readings were taken in the machine itself using a carefully mounted dial gage so that the calibration would be more reliable. The calibration curve (Fig. 13) is linear up to about 30×10^{-3} in. Buckling usually took place at a lower value so that on the test records a straight line up to the displacement corresponding to P_{max} could theoretically be expected.

For the calibration of the midpoint bending strain the readings on the BLH SR-4 Strain Indicator were simply compared with the readings of the oscilloscope. Three curves were taken for different settings of the amplifier attenuator (Fig. 15).

The recorded sine wave serving as a time signal allowed the determination of the time scale: 1 subdivision of the oscilloscope screen corresponded to 0.404 msec.

5. PRELIMINARY TEST SERIES

Preliminary tests were made in order to detect any possible deficiencies of thetest machine and to get some experience in running the tests.

In a first preliminary series, load and head displacement were recorded. It was intended to investigate among other things the consistency of results obtained with three columns of 8.5 in. length and approx. 0.01 eccentricity, three columns of 7.5 in. length and approx. 0.005 eccentricity and three columns of 6.5 in. length and approx. 0.06 eccentricity. Only the end faces of the columns were machined. In order to avoid electronic noise originating in the motor the machine was first run at full speed, the power disconnected and the column loaded at a speed close to its maximum. Thus the speed was comparable with that of the later tests in which the power was kept on.

The analysis of the photographic records gave the head displacement δ, and thus the head velocity c and the maximum load P_{max}. The dynamic similarity number Ω as a function of c and column length L was taken from Fig. 21. The Euler load P_E from Table 1 together with P_{max} led to the load factor α_{max}. The eccentricity e had been obtained earlier by means of a Southwell plot; together with Ω it allowed the determination of the theoretical load factor $\alpha_{max\,th}$ from Fig. 18 which is a careful reproduction of Fig. 5 of Ref. (3). The results obtained as shown in Fig. 18 and Table 2 seem to be in fairly good agreement with theory. No higher consistency was to be expected because the machine was not run at exactly the same speed in each test. Even when movement of the bottom (to be discussed later) was taken into account, the experimental results were slightly low for unknown reasons.

An interesting feature of the displacement curve was noticed. It consisted of two portions, one ranging from the start of loading up to buckling, the other with higher velocity from buckling to the maximum cam displacement. Apparently the machine was slowed down during the buckling process. The change of slope however could be partially due to elasticity of the plunger-spacer system and the flywheel bearings, but these were estimated to be negligibly small in comparison with the change observed. The change of slope was therefore taken to be due to a reduction of speed. The energy absorbed by the column could not account for this, but the cam friction could quite easily do so. Even with a friction factor of 0.01 the work done would be many times that absorbed by the column. One feature which has not been looked into is the possibility of hydrodynamic action in the grease film between cam and plunger. Such a film would have a thickness dependent on the load and would appear as an elasticity of the system. It should be mentioned that all recorded velocities were markedly lower than those which would theoretically correspond to the measured flywheel speed. Whatever the exact reasons for these particular features of the displacement curves, the recorded displacements could be regarded as correct for the upper column end. Thus whereas the movement of the upper column end was known there were some doubts with respect to the movement of the lower end.

Subsequently measurements were made which clearly showed that for the range of the maximum loads encountered in our tests there was a displacement of the bottom piece equal to approximately 2.2×10^{-3} in. and varying slightly over the range of loads (see Fig. 14) . The variation was considered negligibly small with respect to the total head displacement. The measurements were taken by means of the load transducer and a dial gage reading in 10^{-4} in.

For the projected main tests it was intended to record load and midpoint bending strain which would allow the determination of the maximum strain at the inner midpoint of the column. As there was only a dual-beam oscilloscope available, the recording of the head displacement had to be abandoned. This could be done as it was intended to run the future tests at constant maximum speed which also meant, at least theoretically, at constant maximum head velocity. For verification,

possible relations between actual head velocity and eccentricity and column length had to be investigated. It turned out that eccentricity did not affect the head velocity, column length however did.

Subsequently another preliminary test series of ten columns was made which clearly showed that the actual head velocity decreased slightly with column length. Because of the relatively high scatter a straight line was computed by the method of least squares that served as a basis for the main test series (see Fig. 16 and Table 3) . In evaluating the actual head velocity, the movement of the bottom was taken into account. For the two main test series the head velocities given in Table 5 were computed from the above mentioned line for the various column lengths. The flywheel rotational speed and its theoretically related head velocity were determined for comparison with the actual head velocity. The former was measured by two different means:

(a) Motor speed and pulley drive ratio:

Motor speed 1860 rpm
Pulley ratio 1:1.2
Thus the flywheel velocity N becomes: N = 2230 rpm

(b) Speed indicator: The number of rotations over one minute was determined several times. On the average the same flywheel velocity was obtained. Thus we have N = 2230 rpm

The relation to the column head velocity:

The cam extends over an angle of $\phi = 60^{\circ}$ and rises linearly with ϕ up to 50×10^{-3} in.

Then

$$c = \frac{\delta_{max}}{t_{max}}$$

where

$$\delta_{max} = 50 \times 10^{-3} \text{ in.}$$

and

$$t_{max} = \frac{10}{N} \text{ sec}$$

This leads to the following formula:

$$c = 5 \times 10^{-3} \, N \text{ in./sec}$$

or with the above value for N :

$$c_{max} = 11.15 \text{ in./sec}$$

6. MAIN TEST SERIES

The general test procedure was described earlier. In the main Test Series No. 1 ten columns were tested. Their length ranged from 6.25 to 8.50 in.; the end faces and the wider sides were machined and the eccentricity was set as close as possible to $e = 0.1$. In Test Series No. 2 ten columns of the same kind were tested; however, the eccentricity aimed at was $e = 0.01$. As mentioned before, with these series besides the load P the midpoint bending strain ϵ_b was recorded instead of the head displacement.

The analysis of the oscillograms led to the maximum load P_{max} and the midpoint bending strain ϵ_b. The Euler load P_E taken from Table 1 together with P_{max} gave the load factor α_{max}. Head velocity c from Table 5 and column length L allowed the determination of Ω through use of Fig. 21. The eccentricity e, obtained previously from a Southwell plot, and Ω led to the theoretical load factor α_{maxth} using interpolation in Fig. 18. In order to get a comparative idea of the agreement between experiment and theory $\alpha_{maxth}/\alpha_{max}$ was computed (see Tables 7 and 9). The analysis of the bending strain curves was rather difficult as they had very high slopes. Furthermore the time at which P_{max} occurred was not always well determined. This explains the scatter in the values of ϵ_b. The mean compressive strain $\bar{\epsilon} = P_{max}/EA$ was easily computed from P_{max}. The total strain ϵ_{tot} at the inner midpoint, the location of highest strain, was then given by $\bar{\epsilon} + \epsilon_b$. Of course high scatter was to be expected for ϵ_{tot} because of ϵ_b (see Tables 8 and 10).

As the experimental results for the load factor could be compared with the theoretical ones given in Ref. (3), it became desirable to have a similar check for the total inner midpoint strain. Steps were taken to have them computed and recorded for the range of parameters of our tests by a YUBA Analogue Computer of the Stanford Electrical Engineering Department. For the computation of the total inner midpoint strain the equation of motion of the column had to be changed into a simple form.

At the same time the variables had to be chosen in a way that their order of magnitude met the requirements of the computer to get the most accurate results possible. The block diagram used for the analogue computer is shown in Fig. 26. As shown in the Appendix for the computation of ϵ_{totth} it was necessary to compute the load factor α. This was recorded at the same time as ϵ_{totth} and very good agreement was obtained with Fig. 5 of Ref. (3).

Computer results for ϵ_{totth} are given in Table 4 and are plotted versus Ω in Fig. 17. This figure served as a basis for Table 6 used for the main Test Series. Figure 25 shows a typical computer record.

7. RESULTS AND ERROR EVALUATION

The experimental and theoretical results for the load factor were plotted and connected by straight lines in Fig. 18 which was obtained by carefully redrawing Fig. 5 of Ref. (3). As can be seen from the figure, fairly good agreement was achieved between theory and experiment. The experimental values are slightly low for unknown reasons. It might be conjectured that there was an influence of plasticity, but as the maximum strains were not much different from the yield limit no definite conclusion can be drawn. As to the scatter, no higher accuracy can be expected in such tests. This is clearly shown by the error evaluation given below.

For the total inner midpoint strain the experimental and theoretical results, the latter as given by the computer, are plotted and connected by straight lines in Figs. 19 and 20. Despite the high scatter for which reasons were given above, sufficiently good agreement was obtained, between theory and experiment.

As it is interesting to know what accuracy can be expected from such experimental investigations and how reliable are the results, a rough error evaluation was made and is presented here. The errors in the values of α_{max} and ϵ_{tot} have different sources like head velocity scatter, eccentricity repeatability, errors in reading oscillograms, errors of calibration and reproduced charts, errors in reading and interpolating charts, and to a smaller extent variations in strain gage power supply and electronic noise.

Only the results of the two main Test Series are considered and the mean value of L is taken as 3.375 in. and that of c as 7.69 in./sec The following error sources were assumed:

Test Series	No. 1	No. 2
For head velocity scatter (see Fig. 16)	±0.8	±0.8 in./sec
For eccentricity repeatability	±0.004	±0.001
or	±4.0 %	±10.0 %

The errors in the values of α_{max} and ϵ_{tot} due to these error sources were determined through use of Figs. 17 and 18 and were found to be:

Test Series	No. 1	No. 2
For the load factor	±8.5 %	±9.5 %
For the total inner midpoint strain	±4.0 %	±6.0 %

In evaluating the error in the calculated value of ϵ_{tot} the error in the value of $\bar{\epsilon}$ (assumed to be the same as that in the value of α_{max}) was taken into account in proportion to its contribution to ϵ_{tot}. For the complete analysis (errors in reading oscillograms, errors of calibration and reproduction of charts, errors in reading and interpolating charts) the following errors as percentages were evaluated:

Test Series	No. 1	No. 2
For the load factor	±2.0 %	±3.0 %
For the total inner midpoint strain	±16.5 %	±16.5 %

Introduction of an error due to variation of strain gage power supply and electronic noise of ±0.5 % results in the following total errors as percentages:

Test Series	No. 1	No. 2
For the load factor	±11.0 %	±13.0 %
For the total inner midpoint strain	±21.0 %	±23.0 %

It can be verified that all the experimental results lie in the quoted error range.

V. CONCLUSIONS

As shown by the test results, the maximum strains attained (see Figs. 19 and 20) were very close to the yield limit of the material of the column and partly in the plastic region which was the goal of the investigation. The results have also shown that, in principle, there are two means to get still further into the plastic range: one is to decrease the eccentricity which is difficult to do and would be at the expense of accuracy, and the other to increase the dynamic similarity number. This could be achieved either by decreasing the slenderness ratio, which would reduce the dynamic influence and increase the load beyond the capacity of the machine, or by increasing the head velocity, which is limited by the performance of the testing machine. As to the testing machine it was found that it could hardly be improved further beyond the final state in which it was used in the present experiments. For future tests a more rigid and better balanced, slightly bigger machine (to permit a more accurate adjustment of the columns) with a higher number of revolutions should be used. Another means by which to get further into the plastic range would be to select a material with a lower yield limit.

APPENDIX

ANALOGUE COMPUTER ANALYSIS

The equation of motion in terms of a non-dimensional displacement f and a non-dimensional displacement ξ is given in Appendix II of Ref. (2) (Eq. 75, p. 39) as follows:

$$\frac{d^2f}{d\xi^2} + \Omega\left[(1 - \xi)f - e + \frac{1}{4}f^3 - \frac{1}{4}e^2 f\right] = 0 \qquad (1)$$

With the substitutions

$$f = ay \quad \text{and} \quad \xi = bx \qquad (2)$$

the differential equation of motion can be given as:

$$\frac{d^2y}{dx^2} - \Omega b^3\left[\left(x - \frac{1 - \frac{e^2}{4}}{b}\right) - \frac{a^2}{4b}y^2\right]y = e\,\Omega\,\frac{b^2}{a} \qquad (3)$$

At this point the values of a and b can still be chosen arbitrarily. Since the computer voltage range was from 0 to 100 V, a suitable value for b was taken to be such that

$$\frac{1 - \frac{e^2}{4}}{b} = 10 \qquad (4)$$

Then

$$b = \frac{1 - \frac{e^2}{4}}{10} = C^2 \qquad (5)$$

and from Eq. (2)

$$\xi = \frac{1 - \frac{e^2}{4}}{10}x = C^2 x \qquad (6)$$

where

$$C = \sqrt{\frac{1 - \frac{e^2}{4}}{10}} \qquad (7)$$

When this value of b is inserted in the bracketed expression of Eq. (3) it leads to the equation

$$\frac{d^2y}{dx^2} - \Omega\, b^3 \left[(x - 10) - \frac{5a^2}{2\left(1 - \frac{e^2}{4}\right)} y^2 \right] y = e\, \Omega\, \frac{b^2}{a} \tag{8}$$

Now a value for the coefficient of y^2 involving a in the brackets can be chosen in order to determine a. Take

$$\frac{5a^2}{2\left(1 - \frac{e^2}{4}\right)} = \frac{1}{100} \tag{9}$$

Then

$$a = \frac{1}{5}\sqrt{\frac{1 - \frac{e^2}{4}}{10}} = \frac{C}{5} \tag{10}$$

and from Eq. (2)

$$f = \frac{1}{5}\sqrt{\frac{1 - \frac{e^2}{4}}{10}} \cdot y = \frac{C}{5}\, y \tag{11}$$

When this value of a is inserted in Eq. (8) the result is

$$\frac{d^2y}{dx^2} - \left(\frac{1 - \frac{e^2}{4}}{10}\right)^3 \Omega \left(x - 10 - \frac{y^2}{100}\right) y = 5 \left(\frac{1 - \frac{e^2}{4}}{10}\right)^{3/2} e\, \Omega$$

or

$$y'' = C_1 \left(x - 10 - \frac{y^2}{100}\right) y + C_2 \tag{12}$$

where

$$C_1 = \left(\frac{1 - \frac{e^2}{4}}{10}\right)^3 \Omega = C^6\, \Omega \tag{13}$$

$$C_2 = 5 \left(\frac{1 - \frac{e^2}{4}}{10}\right)^{3/2} e\, \Omega = 5\, C^3\, e\, \Omega \tag{14}$$

and where the prime indicates differentiation with respect to x. The initial conditions are at $t = \xi = x = 0$:

$$f = e \quad \text{and} \quad \frac{df}{d\xi} = 0$$

It follows from Eq. (11) that at this time

$$e = \frac{1}{5}\sqrt{\frac{1 - \frac{e^2}{4}}{10}}\, y(0) = \frac{c}{5}\, y(0)$$

so that

$$y(0) = \frac{5e}{\sqrt{\frac{1 - \frac{e^2}{4}}{10}}} = \frac{5e}{c} \tag{15}$$

Also, from Eq. (2):

$$y'(0) = 0 \tag{16}$$

The load factor α can now be determined by using the following formula from Appendix II of Ref. (2) (Eq. 76, p. 39):

$$\alpha = \xi - \frac{f^2 - e^2}{4} \tag{17}$$

With the above substitutions the following equation is obtained:

$$\alpha = \left(\frac{1 - \frac{e^2}{4}}{10}\right)x + \frac{e^2}{4} - \frac{1}{100}\left(\frac{1 - \frac{e^2}{4}}{10}\right)y^2$$

or

$$\alpha = \left(\frac{1 - \frac{e^2}{4}}{10}\right)\left(x - 10 - \frac{y^2}{100}\right) + 1 \tag{18}$$

or

$$\alpha = C_3\left(x - 10 - \frac{y^2}{100}\right) + 1 \tag{19}$$

where

$$C_3 = \frac{1 - \frac{e^2}{4}}{10} = c^2 \tag{20}$$

The total inner midpoint strain ϵ_{tot} is given by the following formula (compressive load, stress and strain considered positive):

$$\epsilon_{tot} = \frac{P}{AE} - \left.\frac{d^2Y}{dX^2}\frac{h}{2}\right|_{X = \frac{L}{2}} \tag{21}$$

where all symbols are defined in the Notation. $Y(X)$ is assumed to be of the following form:

$$Y(X) = \rho(f - e) \sin\left(\frac{\pi X}{L}\right) \tag{22}$$

Its second derivative is:

$$Y''(X) = - \rho(\rho - e)\left(\frac{\pi}{L}\right)^2 \sin\left(\frac{\pi X}{L}\right) \tag{23}$$

Thus equation (20) can be expressed as

$$\epsilon_{tot} = \frac{P_E}{AE}\frac{P}{P_E} + \frac{\pi^2}{\left(\frac{L}{\rho}\right)^2}(f - e)\frac{h}{2}\frac{1}{\rho} \tag{24}$$

where

$$\frac{P_E}{AE} = \frac{\pi^2}{\left(\frac{L}{\rho}\right)^2} = \epsilon_E, \quad \rho = \frac{h}{2\sqrt{3}}$$

and

$$\frac{P}{P_E} = \alpha$$

Finally the following simple form is obtained:

$$\epsilon_{tot} = \epsilon_E[\alpha - \sqrt{3}\,(f - e)] \tag{25}$$

Because of Eqs. (11) and (18) Eq. (25) becomes:

$$\epsilon_{tot} = \epsilon_E\left[\frac{1 - \frac{e^2}{4}}{10}\left(x - 10 - \frac{y^2}{100}\right) + 1 + \sqrt{3}\left(\frac{1}{5}\sqrt{\frac{1 - \frac{e^2}{4}}{10}}\,y - e\right)\right] \tag{26}$$

and if

$$\frac{5e}{\sqrt{\frac{1-\frac{e^2}{4}}{10}}} = \frac{5e}{c} = y_o \tag{27}$$

the equation can be written as

$$\frac{5\,\epsilon_{tot}}{\epsilon_E\sqrt{\frac{1-\frac{e^2}{4}}{10}}} = 5\sqrt{\frac{1-\frac{e^2}{4}}{10}}\left(x - 10 - \frac{y^2}{100}\right) + \frac{5}{\sqrt{\frac{1-\frac{e^2}{4}}{10}}} + \sqrt{3}\,(y - y_o) \tag{28}$$

In a simpler form this can be given as

$$C_4\,\epsilon_{tot} = \left[C_5\left(x - 10 - \frac{y^2}{100}\right) + C_6 + \sqrt{3}\,(y - y_o)\right] \tag{29}$$

where

$$C_4 = \frac{5}{\epsilon_E\sqrt{\frac{1-\frac{e^2}{4}}{10}}} = \frac{5}{\epsilon_E c}$$

$$C_5 = 5\sqrt{\frac{1-\frac{e^2}{4}}{10}} = 5c$$

$$C_6 = \frac{5}{\sqrt{\frac{1-\frac{e^2}{4}}{10}}} = \frac{5}{c} \tag{30}$$

In the above formulas the only parameters are the eccentricity e, the dynamic similarity number Ω (as a function of head velocity c and slenderness ratio s) and the Euler strain ϵ_E (as a function of s alone).

The arrangement of the computer to analyse these equations is shown in Fig. 28 as a block diagram.

REFERENCES

1. Erickson, Burton, "Preliminary Design of a High Speed Testing Machine for Column Studies", Thesis Submitted in Partial Fulfillment of the Requirements for the Degree of Master of Science in Applied Mechanics, Polytechnic Institute of Brooklyn, June 1952.

2. Hoff, N. J., "Buckling and Stability; the Forty-First Wilbur Wright Memorial Lecture". Journal of the Royal Aeronautical Society, London, Vol. 58, No. 517, p. 1, January 1954.

3. Erickson, Burton, Nardo, S. V., Patel, Sharad, A., and Hoff, N. J., "An Experimental Investigation of the Maximum Loads Supported by Elastic Columns in Rapid Compression Tests", PIBAL Report No. 296, July 1955; also Proceedings of the Society for Experimental Stress Analysis, Vol. 14, No. 1, p. 13, 1956.

L (in.)	$s = L/\rho$	Ω for $c = 3.16$ in./sec	Ω for $c = 10$ in./sec	P_E (lb)
8.50	117.3	14.42	1.442	922
8.25	113.9	17.22	1.722	991
8.00	110.4	20.74	2.074	1055
7.75	107.0	25.03	2.503	1123
7.50	103.5	30.59	3.059	1199
7.25	100.1	37.35	3.735	1283
7.00	96.6	46.20	4.620	1377
6.75	93.2	57.27	5.727	1480
6.50	89.7	72.11	7.211	1597
6.25	86.3	90.97	9.097	1726

Table 1. Slenderness Ratio, Dynamic Similarity Number and Euler Load for 1/2 x 1/4 in. Columns.

Test No.	L (in.)	e	c (in./sec)	P_{max} (lb)	P_E (lb)	Ω	α_{max}	α_{maxth}	$\frac{\alpha_{maxth}}{\alpha_{max}}$
1	8.5	0.012	7.88	2330	922	2.30	2.53	3.12	1.23
2	8.5	0.009	5.71	2385	922	4.32	2.59	2.83	1.09
3	8.5	0.011	6.20	2445	922	3.65	2.65	2.80	1.06
4	7.5	0.008	6.74	2860	1199	6.60	2.39	2.63	1.10
5	7.5	0.003	7.27	3845	1199	5.80	3.21	2.93	0.91
6	7.5	0.005	6.10	3350	1199	3.80	2.79	3.19	1.14
7	6.5	0.068	6.23	2225	1597	28.50	1.39	1.25	0.90
8	6.5	0.060	6.82	2215	1597	15.40	1.39	1.46	1.05
9	6.5	0.054	4.84	2195	1597	30.50	1.27	1.37	0.93

Table 2. Results of the First Preliminary Test Series.

Test No.	L (in.)	c (in./sec)	$L-\bar{L}$ (in.)	$c-\bar{c}$ (in./sec)	$(L-\bar{L})^2$ ($in.^2$)	$(L-\bar{L})(c-\bar{c})$ ($in.^2$/sec)
1	8.50	7.70	1.125	0.013	1.2656	0.0146
2	8.25	9.05	0.875	1.363	0.7656	1.1926
3	8.00	8.32	0.625	0.633	0.3906	0.3956
4	7.75	7.33	0.375	-0.357	0.1406	-0.0134
5	7.50	8.13	0.125	0.443	0.0156	0.0554
6	7.25	7.71	-0.125	0.023	0.0156	-0.0029
7	7.00	7.53	-0.375	-0.157	0.1406	0.0589
8	6.75	6.76	-0.625	-0.927	0.3906	0.5794
9	6.50	6.83	-0.875	-0.857	0.7656	0.7499
10	6.25	7.51	-1.125	-0.177	1.2656	0.1991

Center of measured points: $\bar{c} = 7.687$ in./sec

$\bar{L} = 7.375$ in.

Slope of the straight line:

$$m = \frac{\Sigma(L-\bar{L})(c-\bar{c})}{\Sigma(L-\bar{L})^2} = 0.6326$$

Table 3. Computation of the Column Head Velocity as a Linear Function of Column Length from Second Preliminary Test Series.

Ω	$\epsilon_{totth} \times 10^3$ for e = 0.1	$\epsilon_{totth} \times 10^3$ for e = 0.01
1.19	3.35	3.65
1.42	3.41	3.73
1.71	3.43	3.80
2.07	3.49	3.86
2.53	3.60	3.95
3.09	3.55	3.98
3.82	3.68	4.10
4.73	3.80	4.07
5.97	3.72	4.23
7.52	3.77	4.26
9.61	4.01	4.33
12.73	4.05	4.50

Table 4. Computer Results for the Total Inner Midpoint Strain.

L (in.)	c (in./sec)
8.50	8.42
8.25	8.26
8.00	8.09
7.75	7.93
7.50	7.76
7.25	7.60
7.00	7.43
6.75	7.27
6.50	7.10
6.25	6.94

Table 5. Head Velocities Used for the Main Test Series.

L (in.)	$\epsilon_{totth} \times 10^3$ for e = 0.1	$\epsilon_{totth} \times 10^3$ for e = 0.01
8.50	3.46	3.82
8.25	3.52	3.89
8.00	3.59	3.96
7.75	3.66	4.03
7.50	3.72	4.11
7.25	3.80	4.18
7.00	3.87	4.26
6.75	3.94	4.34
6.50	4.03	4.43
6.25	4.11	4.53

Table 6. Theoretical Total Inner Midpoint Bending Strain Usef for the Main Test Series.

Test No.	L (in.)	e	c (in. sec	P_{max} (lb)	P_E (lb)	Ω	α_{max}	α_{maxth}	$\frac{\alpha_{maxth}}{\alpha_{max}}$
1.1	8.50	0.091	8.42	2170	893	1.78	2.43	2.53	1.04
1.2	8.25	0.110	8.26	1950	959	2.25	2.03	2.17	1.07
1.3	8.00	0.101	8.09	2040	1021	2.81	1.99	2.04	1.02
1.4	7.75	0.097	7.93	2120	1087	3.54	1.95	1.95	1.00
1.5	7.50	0.097	7.76	1910	1161	4.53	1.65	1.81	1.10
1.6	7.25	0.100	7.60	2020	1242	5.77	1.63	1.67	1.03
1.7	7.00	0.100	7.43	1960	1333	7.47	1.47	1.57	1.07
1.8	6.75	0.103	7.27	1960	1433	9.53	1.37	1.44	1.04
1.9	6.50	0.099	7.10	2090	1546	12.80	1.35	1.37	1.02
1.10	6.25	0.095	6.94	2240	1671	17.07	1.34	1.31	0.98

Table 7. Results of Main Test Series No. 1 for the Load Factor.

Test No.	$\bar{\epsilon} \times 10^3$	$\epsilon_b \times 10^3$	$\epsilon_{tot} \times 10^3$	$\epsilon_{totth} \times 10^3$
1.1	1.69	2.28	3.97	3.46
1.2	1.52	2.82	4.34	3.52
1.3	1.59	1.66	3.25	3.59
1.4	1.65	2.32	3.97	3.66
1.5	1.48	1.97	3.45	3.72
1.6	1.57	1.97	3.54	3.80
1.7	1.52	2.43	3.95	3.87
1.8	1.52	2.35	3.87	3.94
1.9	1.62	2.05	3.67	4.03
1.10	1.74	2.95	4.69	4.11

Table 8. Results of Main Test Series No. 1 for the Total Inner Midpoint Strain.

Test No.	L (in.)	e	c (in./sec)	P_{max} (lb)	P_E (lb)	Ω	α_{max}	α_{maxth}	$\frac{\alpha_{maxth}}{\alpha_{max}}$
2.1	8.50	0.010	8.42	2850	893	1.78	3.19	3.50	1.10
2.2	8.25	0.010	8.26	3070	959	2.25	3.20	3.33	1.04
2.3	8.00	0.009	8.09	3100	1021	2.81	3.04	3.17	1.04
2.4	7.75	0.009	7.93	2900	1087	3.54	2.67	2.78	1.04
2.5	7.50	0.012	7.76	2640	1161	4.53	2.27	2.56	1.13
2.6	7.25	0.010	7.60	3100	1242	5.77	2.50	2.59	1.04
2.7	7.00	0.009	7.43	3510	1333	7.47	2.63	2.42	0.92
2.8	6.75	0.010	7.27	3110	1433	9.53	2.17	2.20	1.01
2.9	6.50	0.009	7.10	3150	1546	12.80	2.04	2.12	1.04
2.10	6.25	0.010	6.94	3160	1671	17.07	1.89	1.93	1.02

Table 9. Results of the Main Test Series No. 2 for the Load Factor.

Test No.	$\bar{\epsilon} \times 10^3$	$\epsilon_b \times 10^3$	$\epsilon_{tot} \times 10^3$	$\epsilon_{totth} \times 10^3$
2.1	2.21	1.97	4.18	3.82
2.2	2.39	1.86	4.25	3.89
2.3	2.41	1.11	3.52	3.96
2.4	2.25	1.35	3.60	4.03
2.5	2.05	1.83	3.88	4.11
2.0	2.41	1.63	4.04	4.18
2.7	2.73	2.43	5.16	4.26
2.8	2.42	2.50	4.92	4.34
2.9	2.45	2.32	4.77	4.43
2.10	2.46	2.84	5.30	4.53

Table 10. Results of Main Test Series No. 2 for the Total Inner Midpoint Strain .

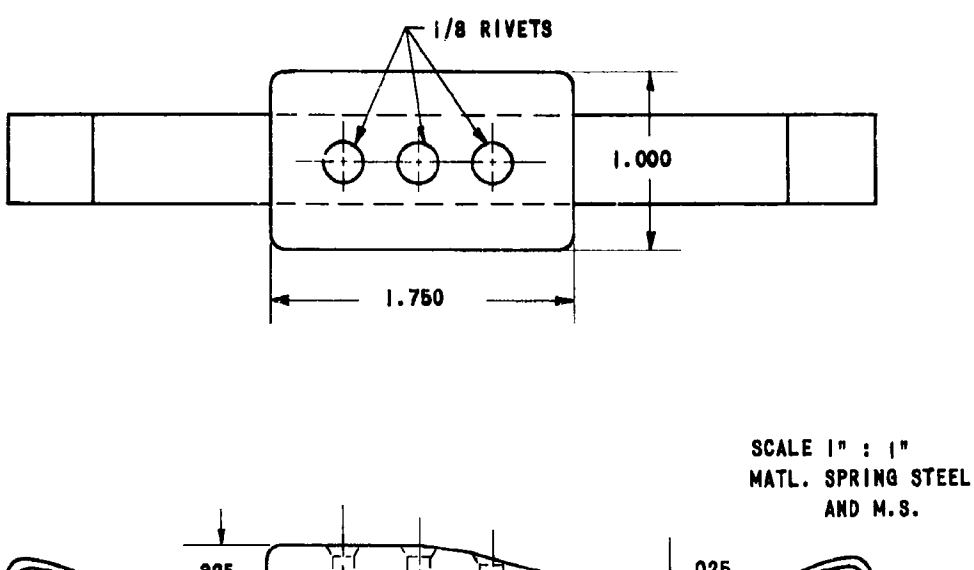

FIG. 1. SPACER.

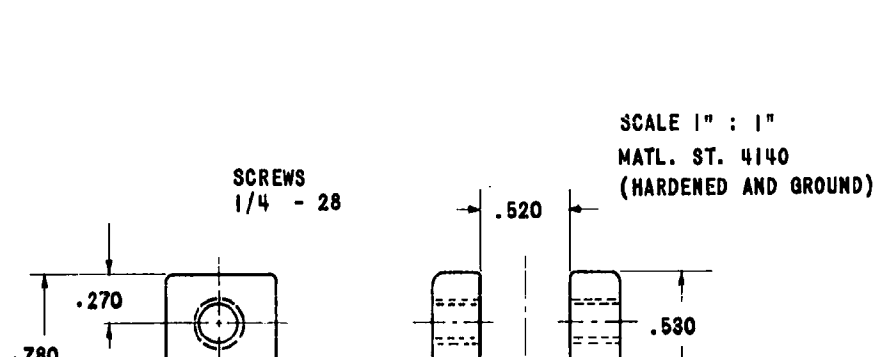

FIG. 2. END PIECES.

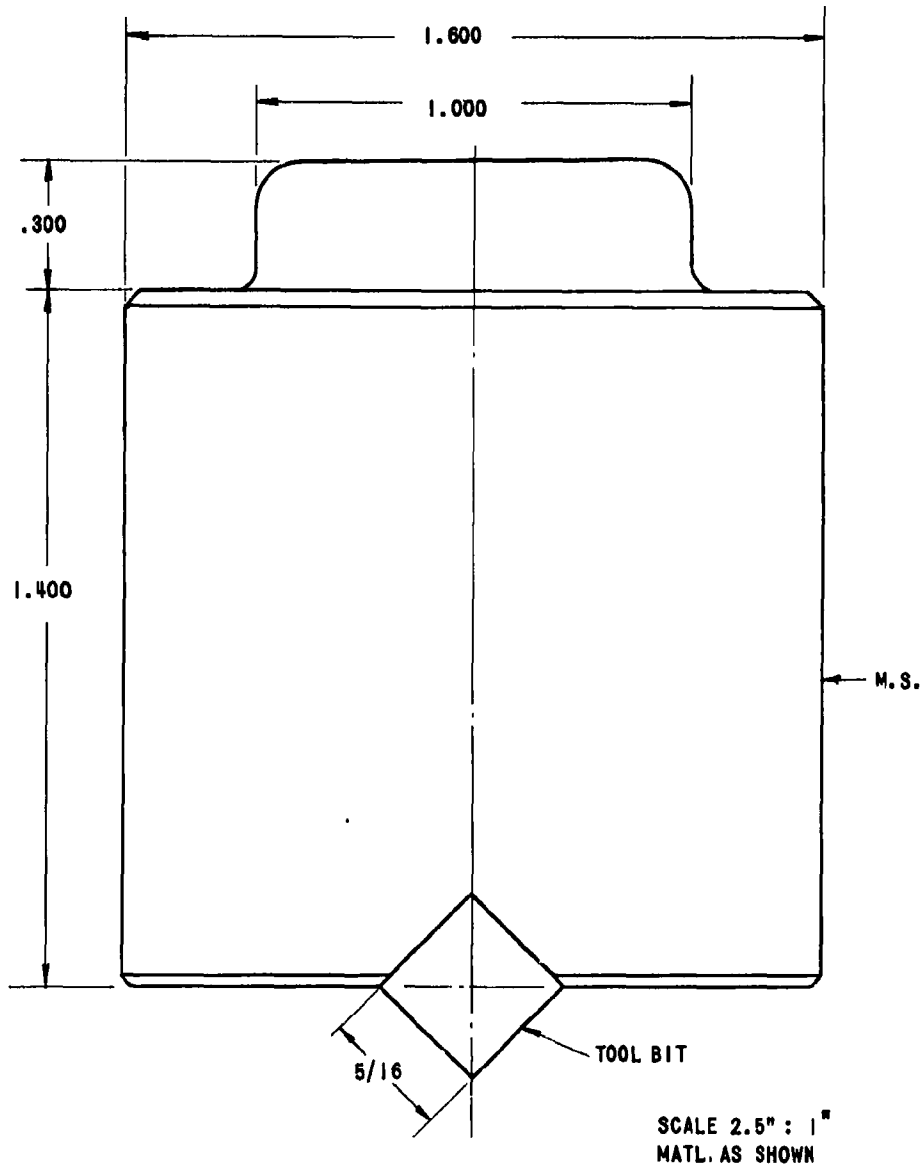

FIG. 3. LOWER PLUNGER CARRYING COLUMN KNIFE EDGE.

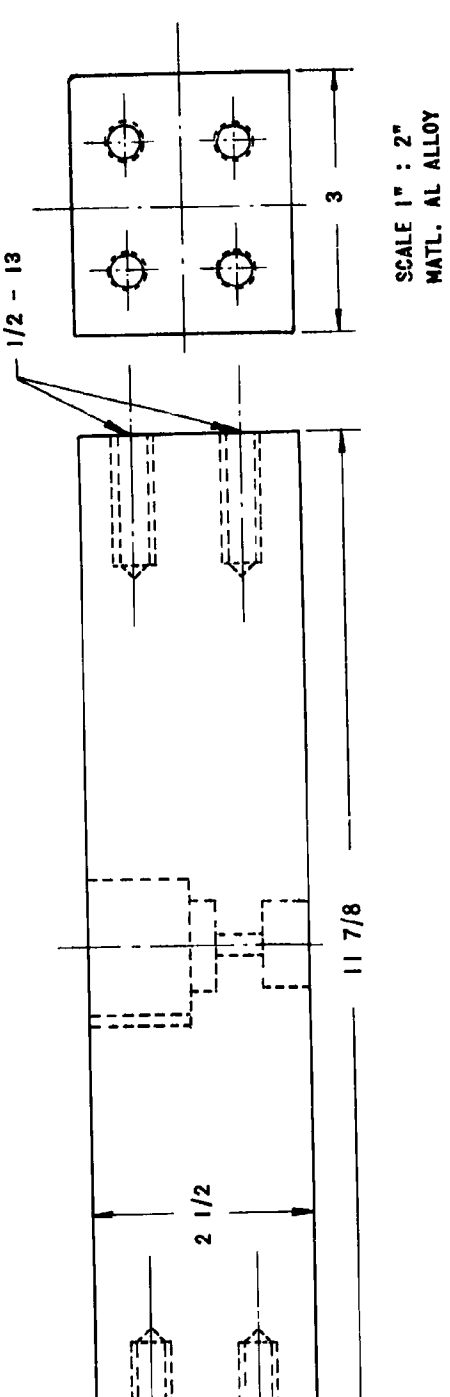

FIG. 4. BOTTOM PIECE.

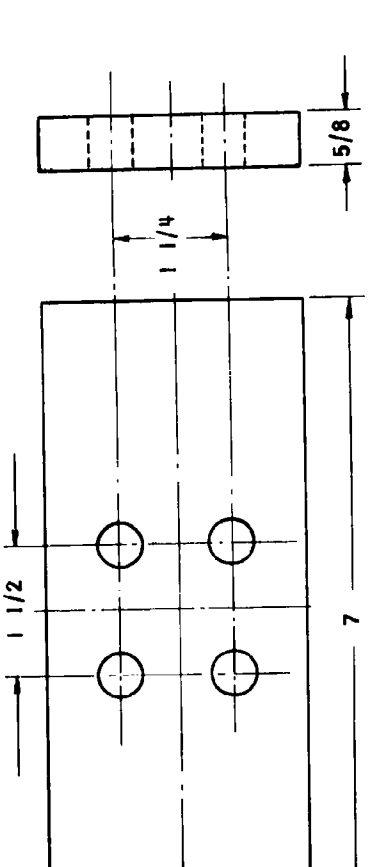

FIG. 5. CLAMPING PLATES.

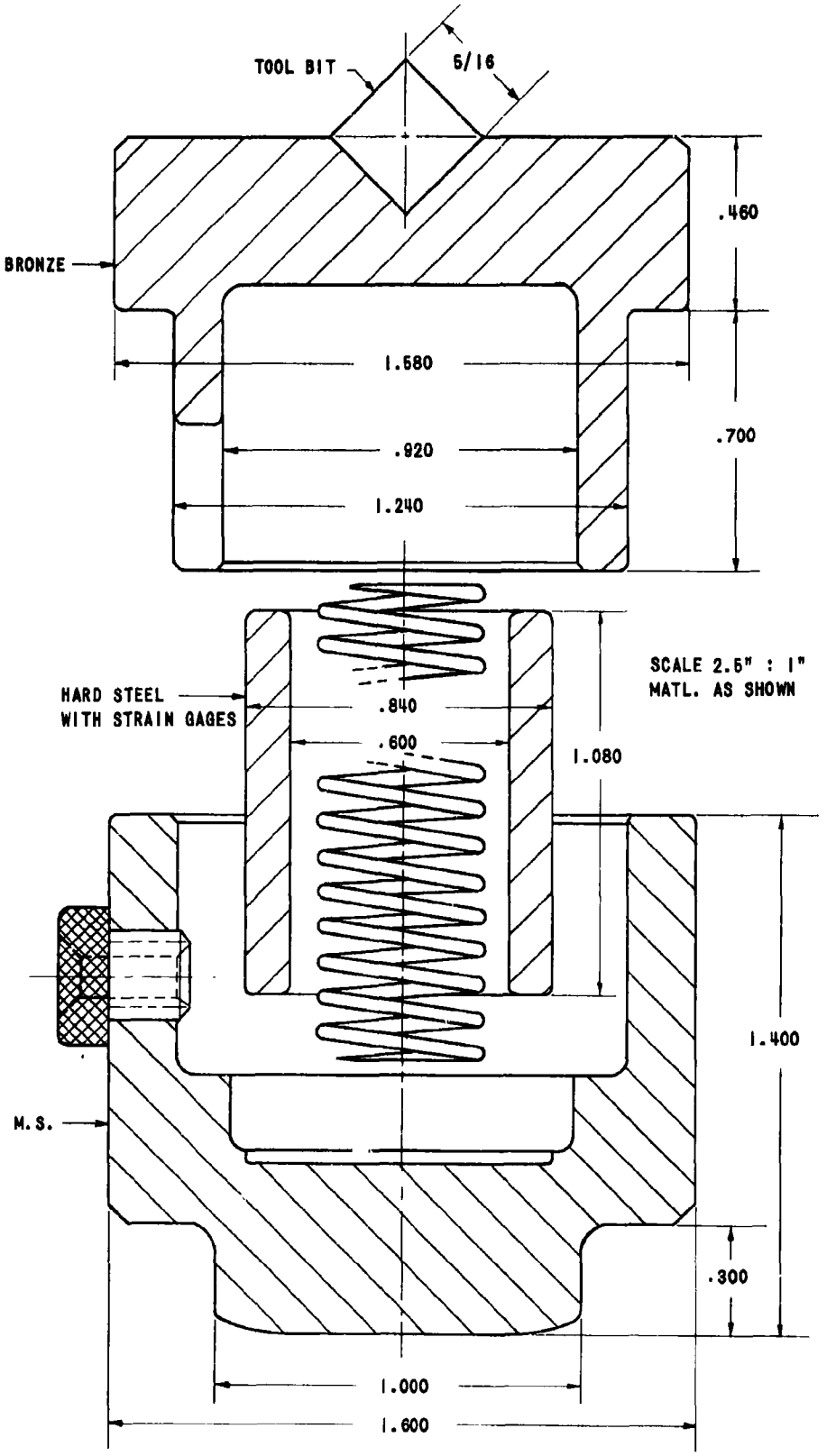

FIG. 6. LOAD TRANSDUCER UNIT.

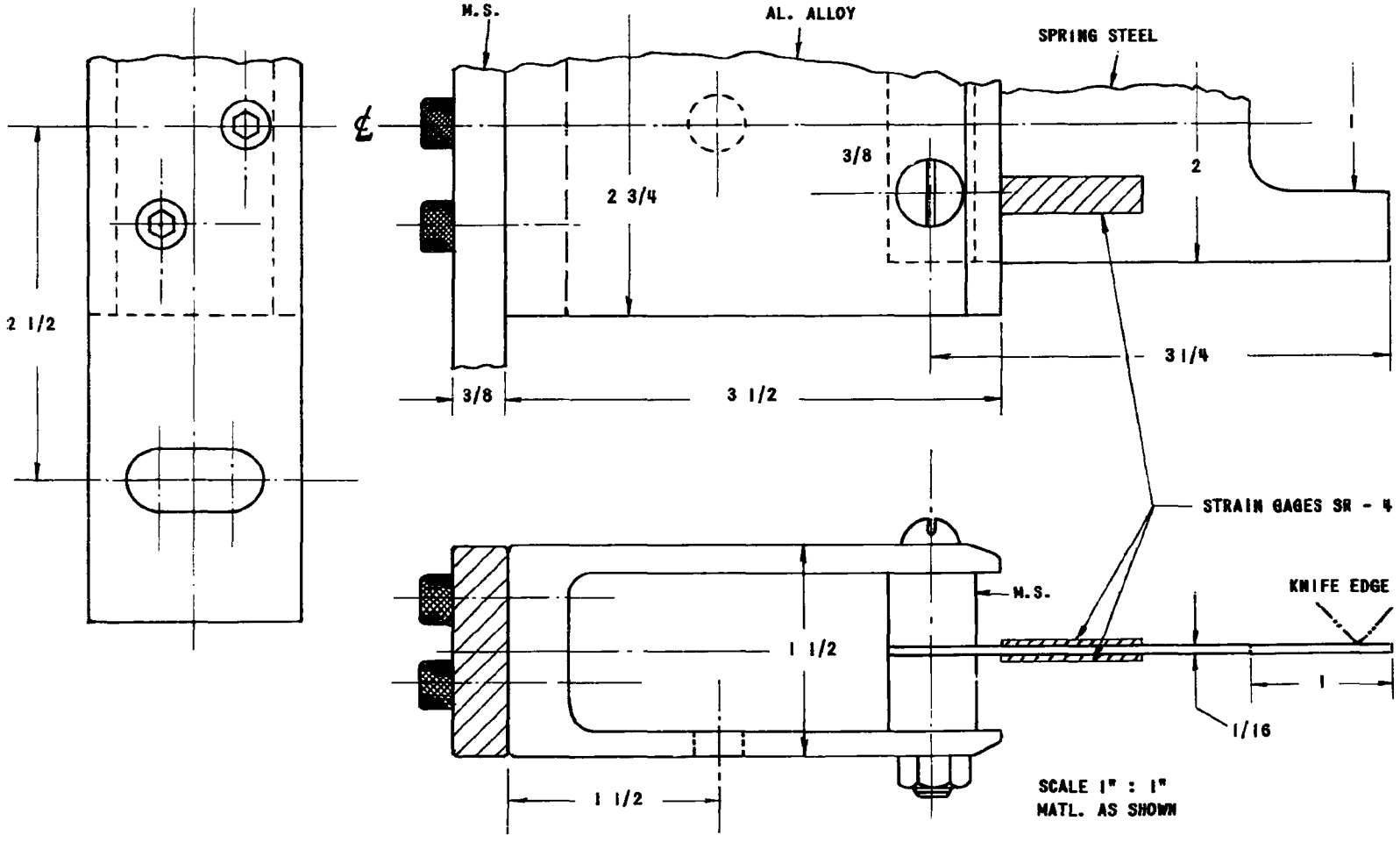

FIG. 7. DEFLECTION CANTILEVER.

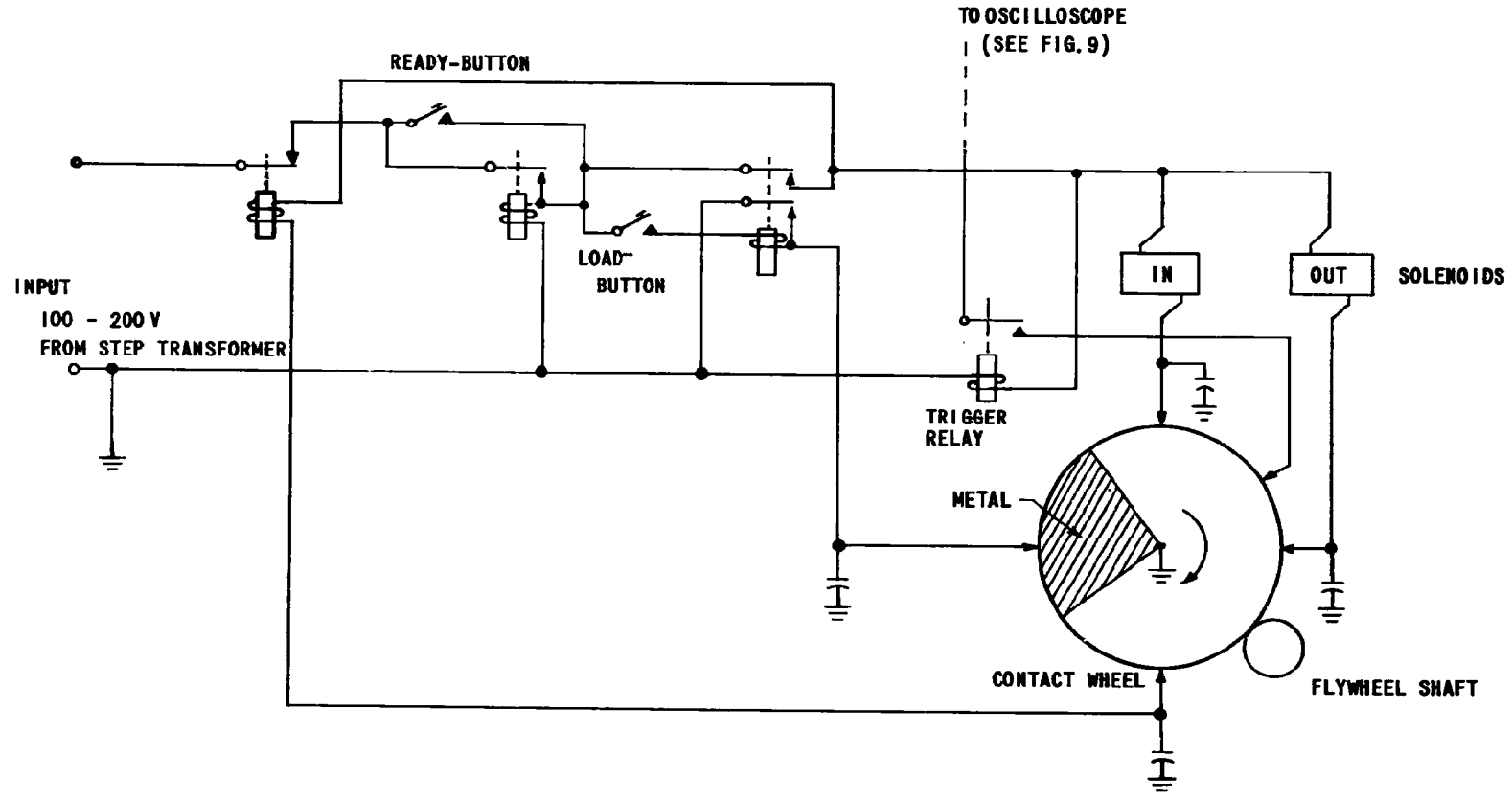

FIG. 8. SYNCHRONIZATION MECHANISM.

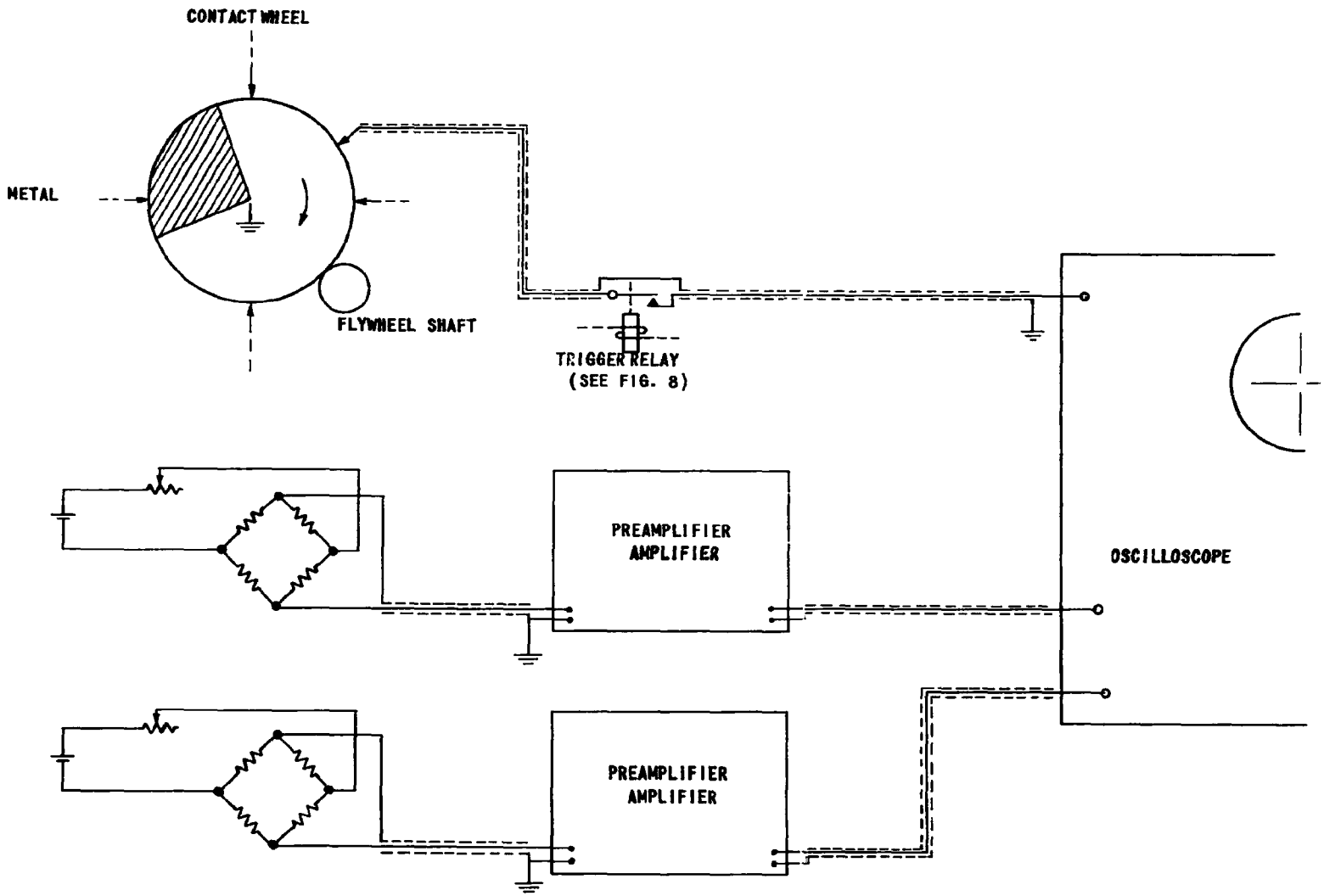

FIG. 9. INSTRUMENTATION

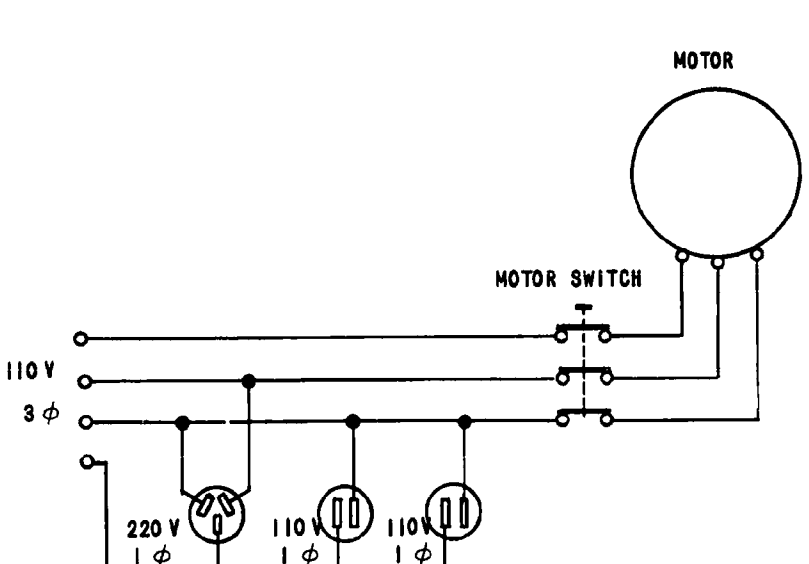

FIG. 10. MOTOR CIRCUIT.

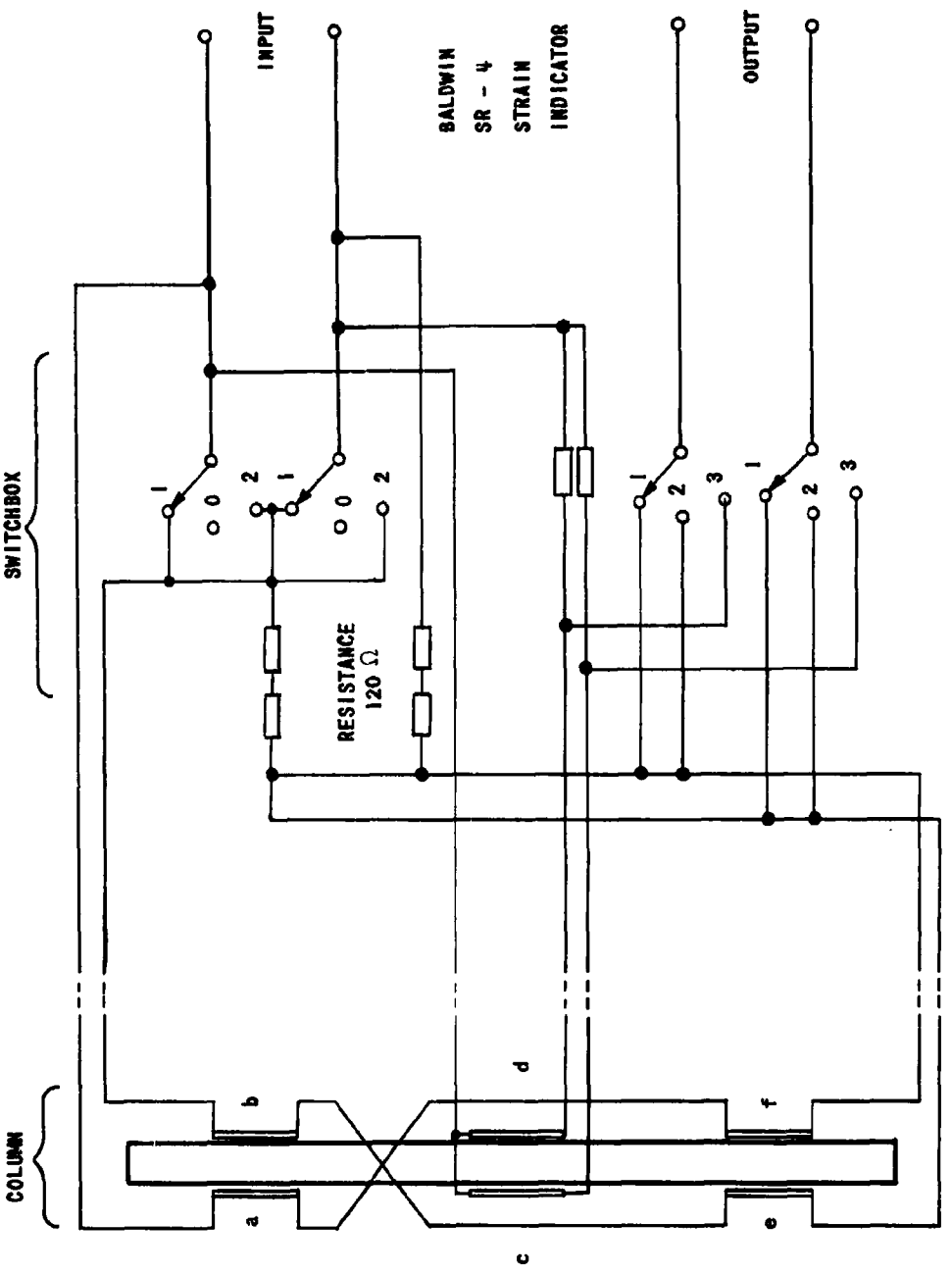

FIG. 11a. COLUMN STRAIN GAGE CIRCUITRY.

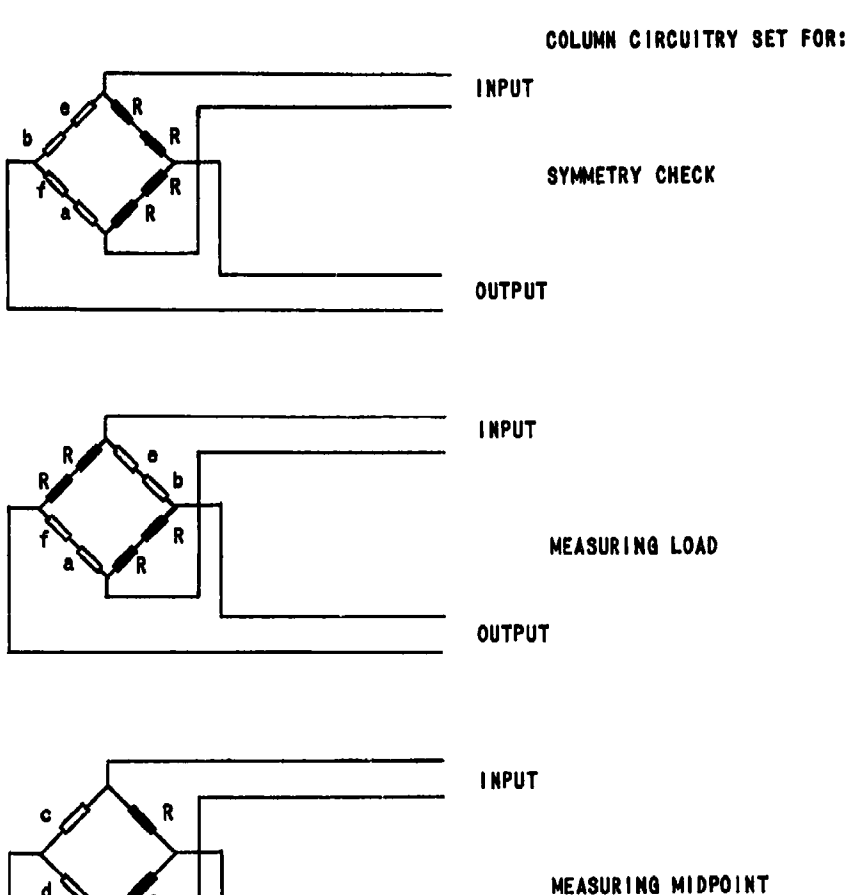

FIG. 11b. SIMPLIFIED COLUMN STRAIN GAGE CIRCUITRY (see Fig. 11a).

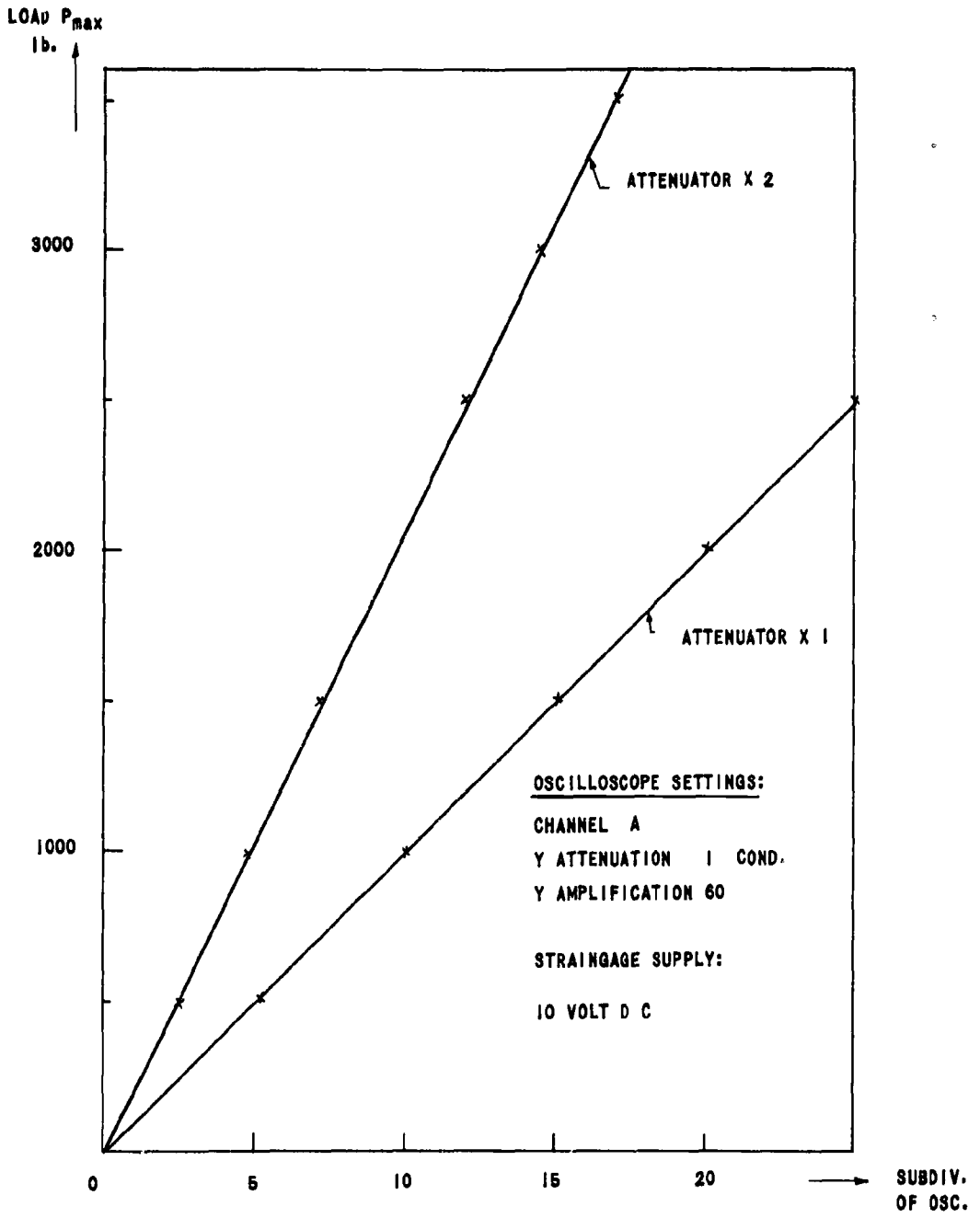

FIG. 12. CALIBRATION LOAD VS OSCILLOSCOPE DEFLECTION.

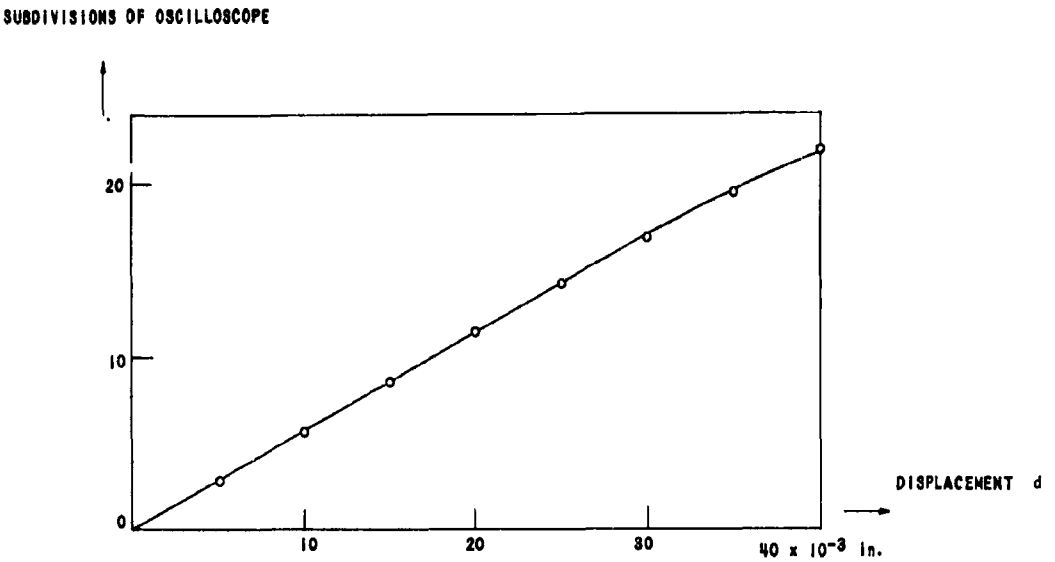

FIG. 13. CANTILEVER BEAM CALIBRATION.

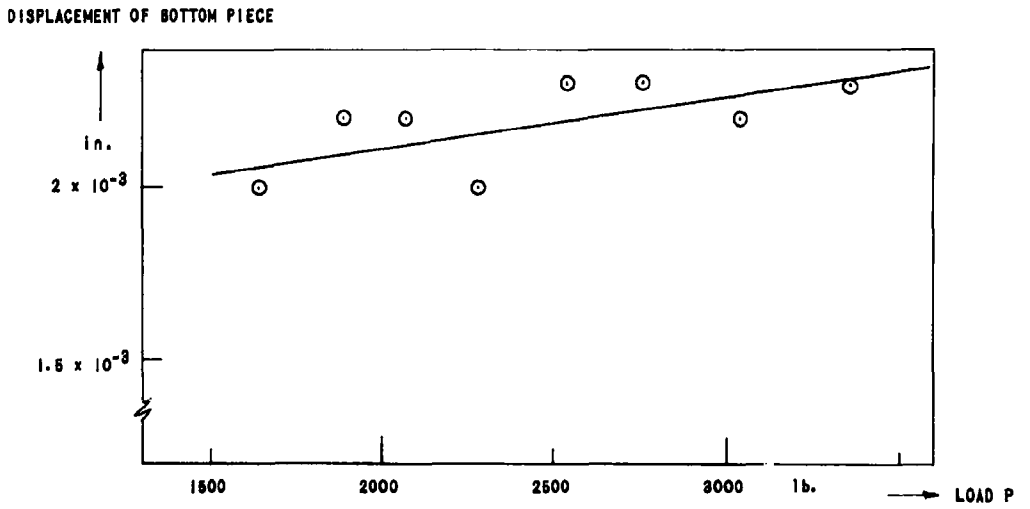

FIG. 14. BOTTOM MOVEMENT VS LOAD.

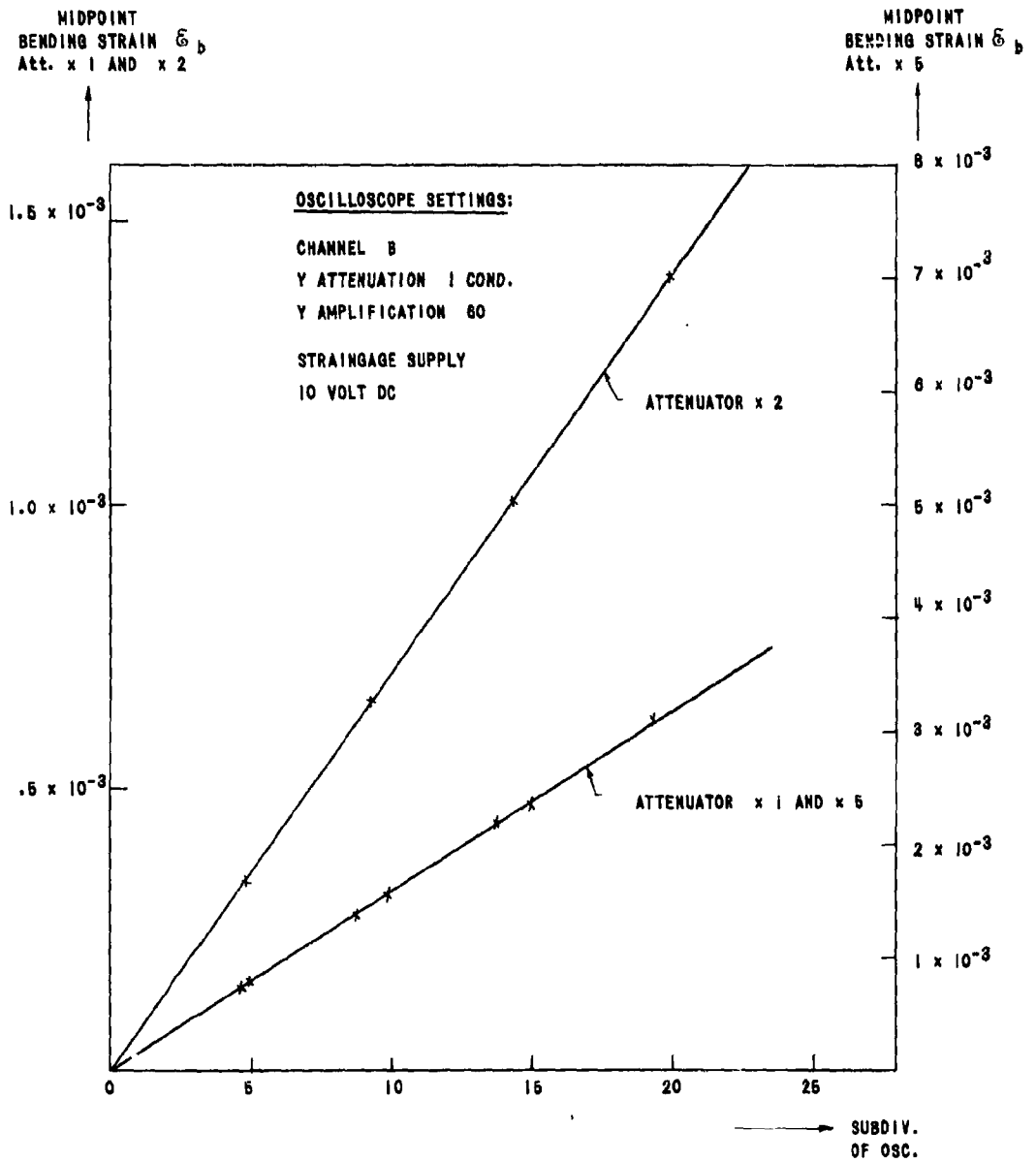

FIG. 15. CALIBRATION BENDING STRAIN VS OSCILLOSCOPE DEFLECTION.

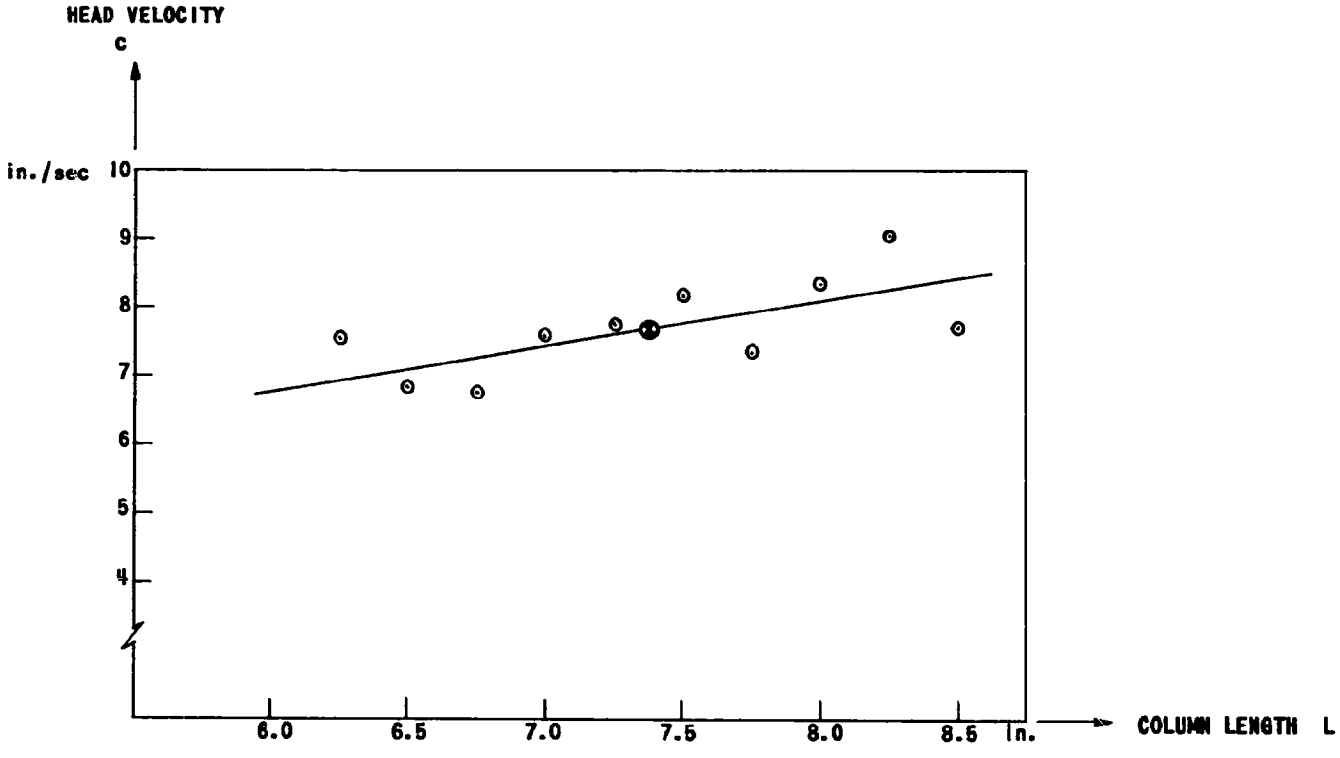

FIG. 16. HEAD VELOCITY VS COLUMN LENGTH.

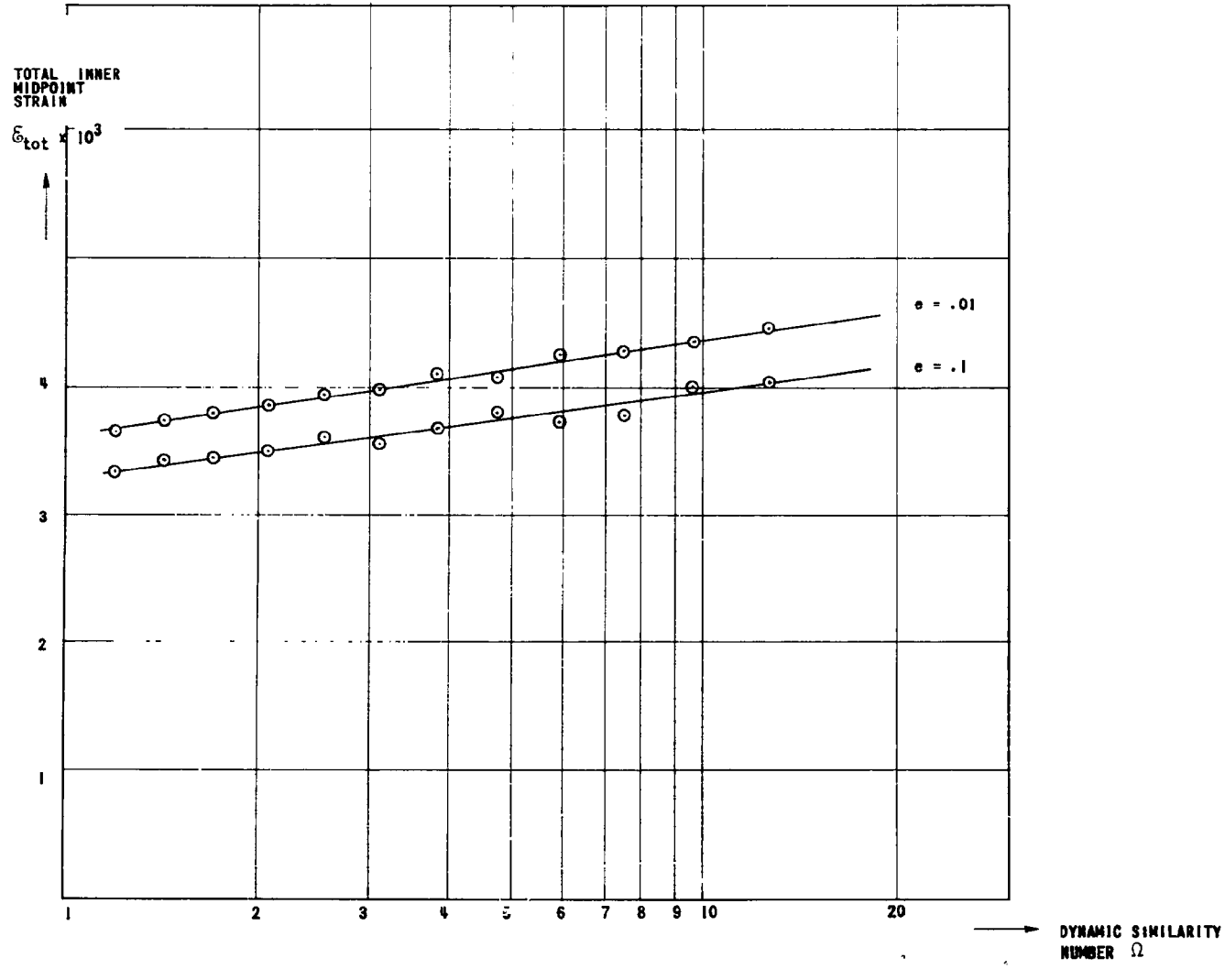

FIG. 17. COMPUTER RESULTS FOR TOTAL INNER MIDPOINT STRAINS AS A FUNCTION OF DYNAMIC SIMILARITY NUMBER.

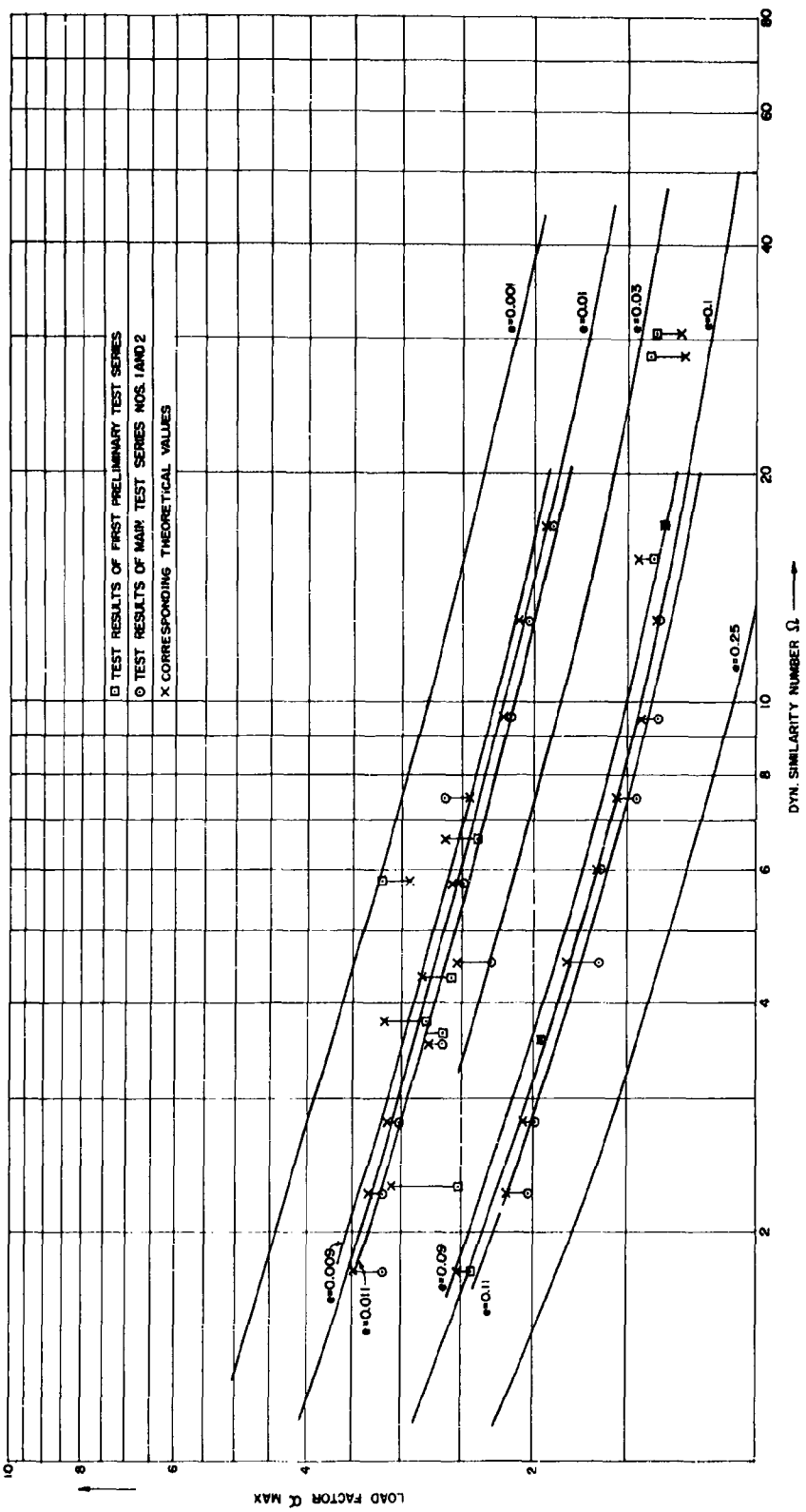

FIG. 18. LOAD FACTOR VS DYNAMIC SIMILARITY NUMBER (curves reproduced from Fig. 5 of Ref. 3).

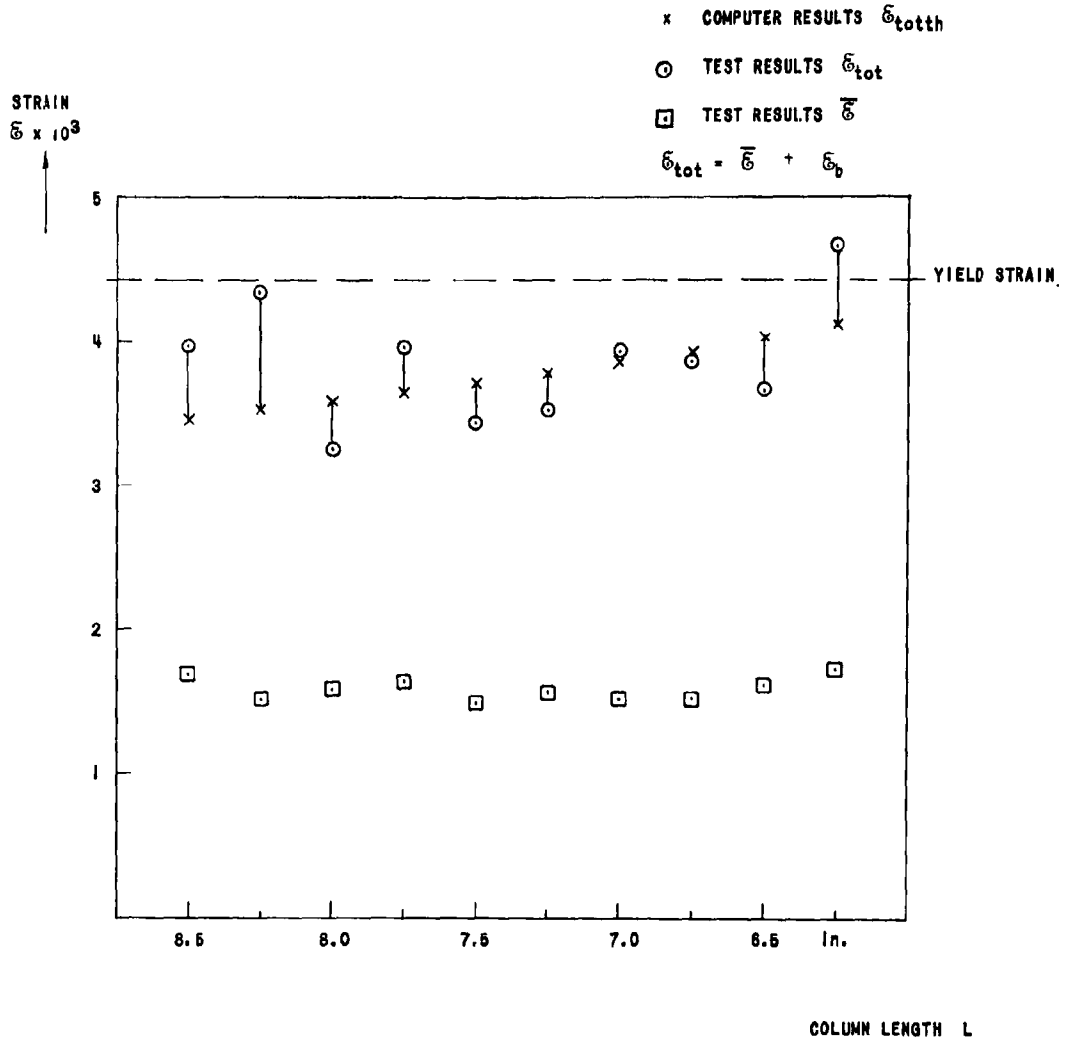

FIG. 19. STRAINS AT INNER MIDPOINT IN TEST SERIES NO. 1.

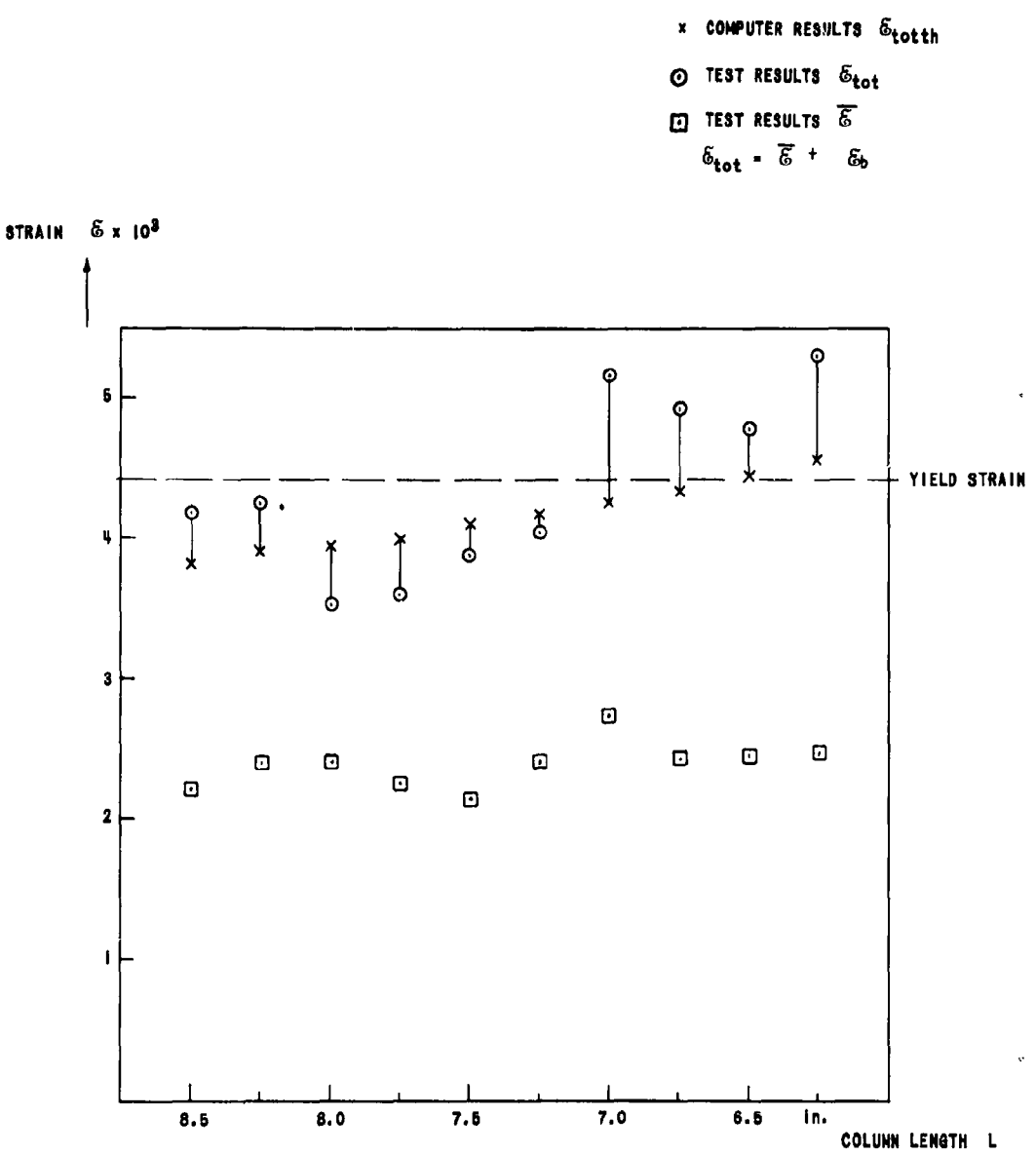

FIG. 20. STRAINS AT INNER MIDPOINT IN TEST SERIES NO. 2.

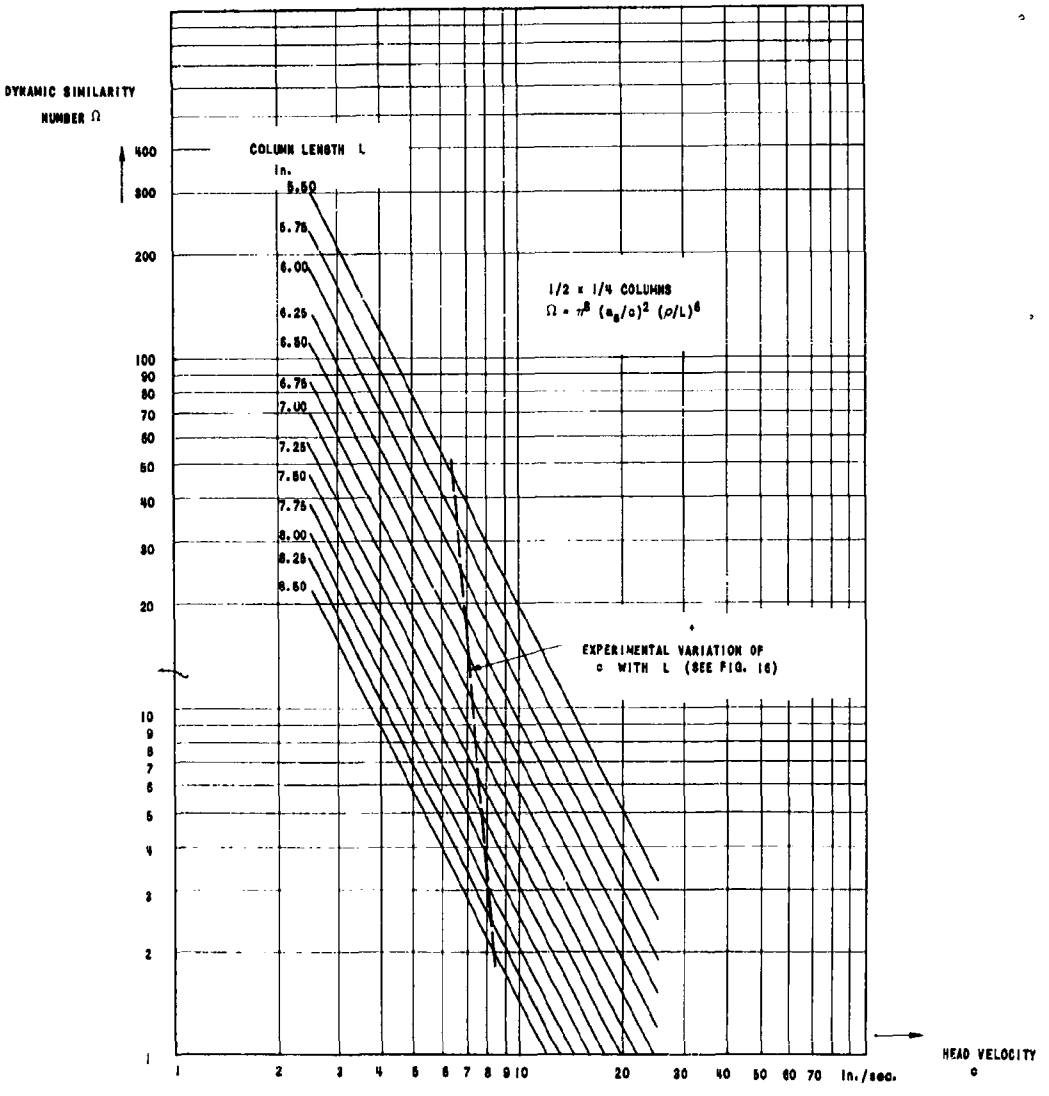

FIG. 21. DYNAMIC SIMILARITY NUMBER VS HEAD VELOCITY.

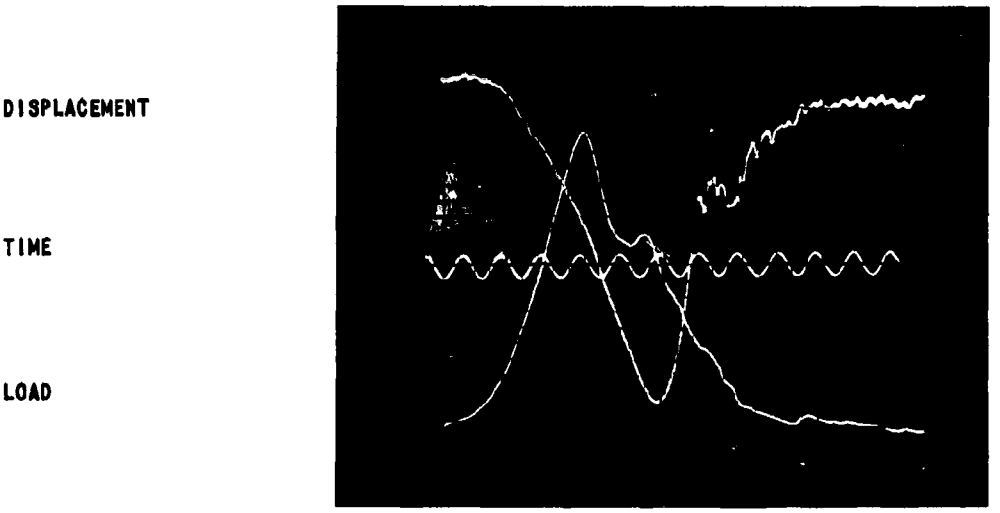

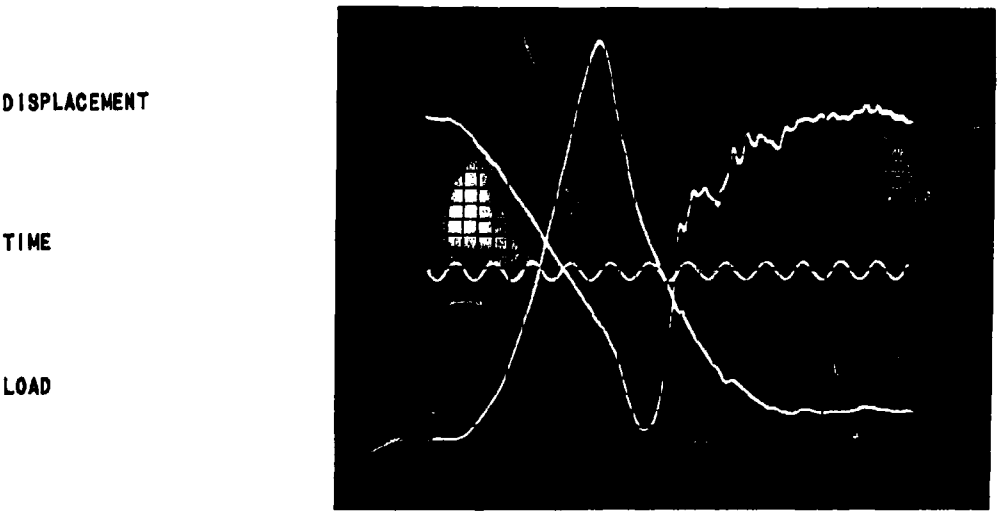

FIG. 22. TWO TYPICAL TEST RECORDS TAKEN FROM PRELIMINARY TEST SERIES.

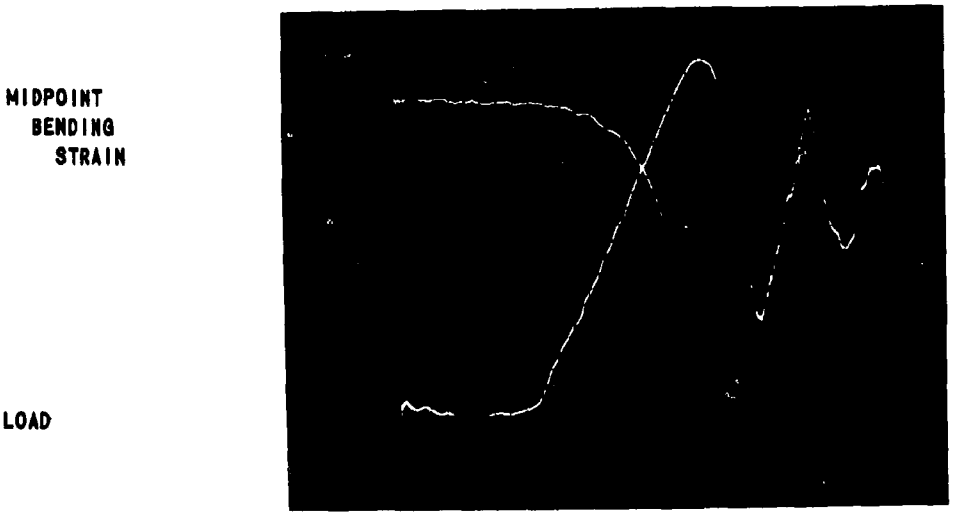

FIG. 23. RECORD OF TEST NO. 1.10 (L/ρ = 87.7, e = 0.095, Ω = 17.1).

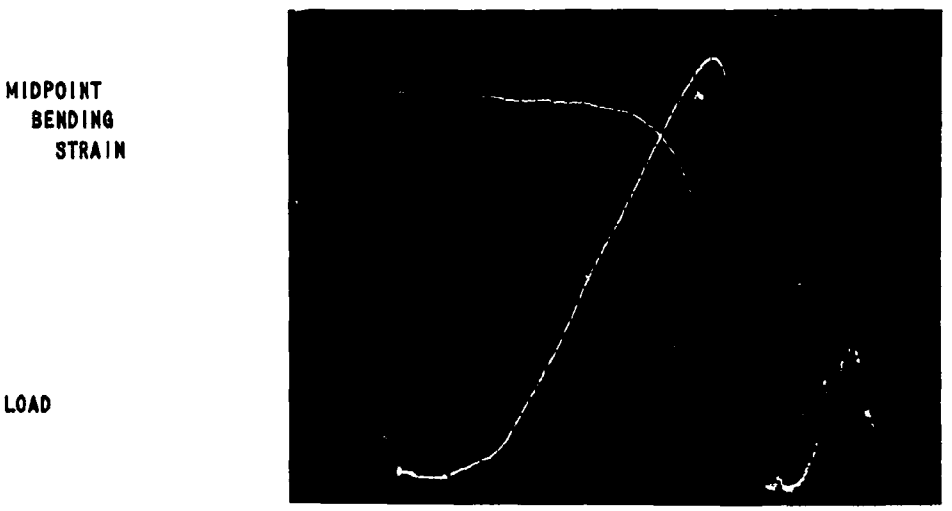

FIG. 24. RECORD OF TEST NO. 2.5 (L/ρ = 105, e = 0.012, Ω = 4.53).

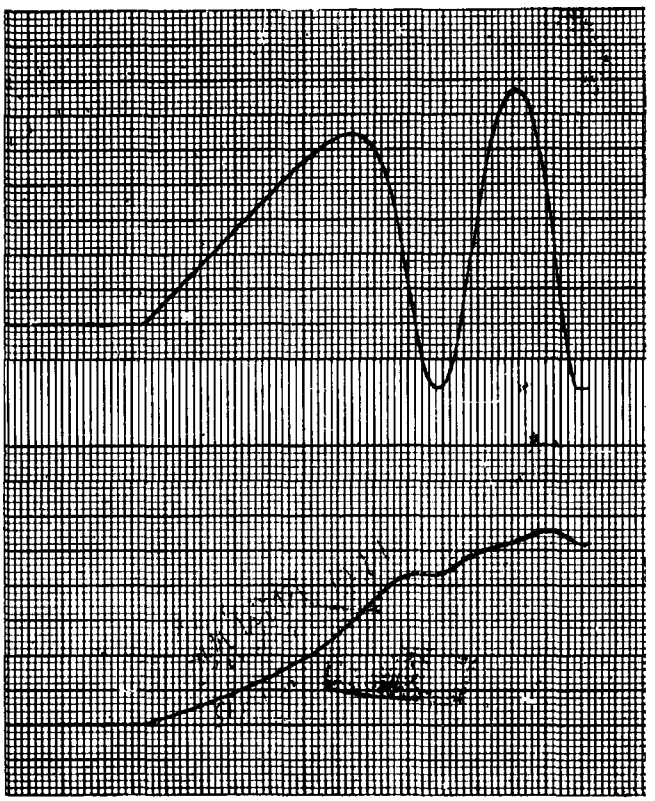

FIG. 25. TYPICAL COMPUTER RECORD.

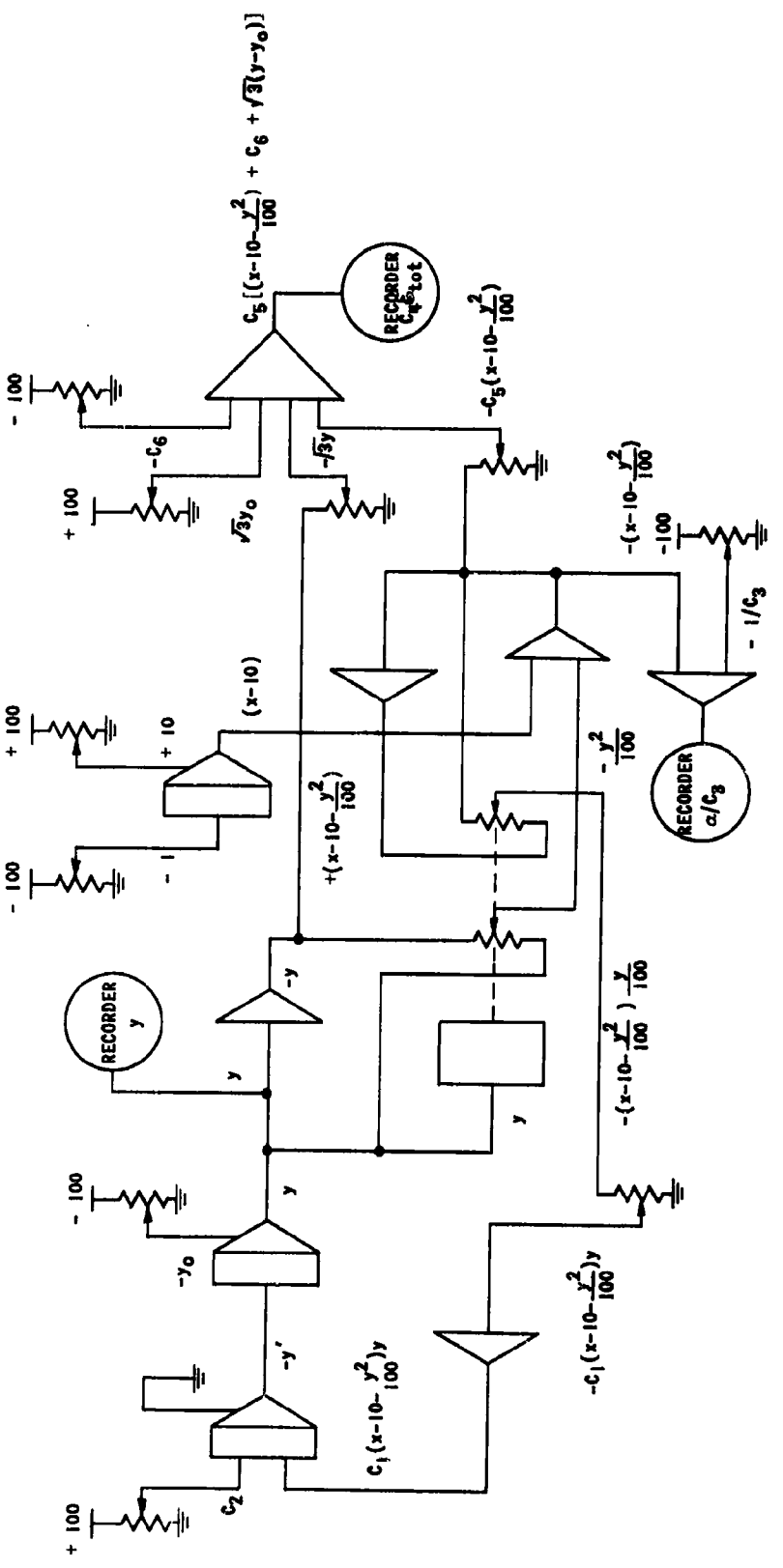

FIG. 26. ANALOGUE COMPUTER BLOCK DIAGRAM.

Distribution List for Unclassified Technical Reports Issued Under Contract Nonr-225(47) Task NR 064-434.

Chief of Naval Research
Department of the Navy (2)
Washington 25, D. C.
Attn: Code 439

Commanding Officer
Office of Naval Research (1)
Branch Office
495 Summer Street
Boston 10, Massachusetts

Commanding Officer
Office of Naval Research (1)
Branch Office
John Crerar Library Building
86 E. Randolph Street
Chicago 11, Illinois

Commanding Officer
Office of Naval Research (1)
Branch Office
346 Broadway
New York 13, New York

Commanding Officer
Office of Naval Research (1)
Branch Office
1030 E. Green Street
Pasadena, California

Commanding Officer
Office of Naval Research (1)
Branch Office
1000 Geary Street
San Francisco, California

Commanding Officer
Office of Naval Research (25)
Branch Office
Navy No. 100, Fleet Post Office

Director
Naval Research Laboratory
Washington 25, D. C.
Attn: Tech. Info. Officer (6)
Code 6200 (1)
Code 6205 (1)
Code 6250 (1)
Code 6260 (1)

Armed Services Technical Information
Agency (10)
Arlington Hall Station
Arlington 12, Virginia

Office of Technical Services
Department of Commerce (1)
Washington 25, D. C.

Director of Defense Research and Engineering
The Pentagon (1)
Washington 25, D. C.
Attn: Technical Library

Chief, Defense Atomic Support Agency
The Pentagon
Washington 25, D. C.
Attn: Technical Information Division (2)
Weapons Effects Division (1)
Special Field Projects (1)
Blast and Shock Branch (1)

Office of the Secretary of the Army
The Pentagon (1)
Washington 25, D. C.
Attn: Army Library

Chief of Staff
Department of the Army
Washington 25, D. C.
Attn: Development Branch (RandD Div. (1)
Research Branch (RandD Div. (1)
Special Weapons Br. (RandD Div. (1)

Office of the Chief of Engineers
Department of the Army
Washington 25, D. C.
Attn: ENG-HL Lib. Br., Adm. Ser. Div. (1)
ENG-WD Planning Div. Civil Wks. (1)
ENG-EB Port. Constr. Br., Eng. Div., Mil. Constr. (1)
ENG-EA Struc. Br., Eng. Div., Mil. Constr. (1)
ENG-NB Special Engr. Br., Eng. RandD Div. (1)

Commanding Officer
Engineer Research Development Laboratory (2)
Fort Belvoir, Virginia

Office of the Chief of Ordance
Department of the Army
Washington 25, D. C.
Attn: Research and Materials
Branch (Ord RandD Div.) (1)

Office of the Chief Signal Officer
Department of the Army
Washington 25, D. C.
Attn: Engineering and Technical Division (1)

Commanding Officer
Watertown Arsenal (1)
Watertown, Massachusetts
Attn: Laboratory Division

Office of Ordnance Research
2127 Myrtle Drive
Duke Station
Durham, North Carolina
Attn: Division of Engineering Sciences (4)

Commanding Officer
Squier Signal Laboratory
Fort Monmouth, New Jersey
Attn: Components and Materials Branch (1)

Chief of Naval Operations
Department of the Navy
Washington 25, D. C.
Attn: Op 91 (1)
Op 03EG (1)

Commandant, Marine Corps
Headquarters, U. S. Marine Corps (1)
Washington 25, D. C.

Commander
Wright Air Development Center
Wright-Patterson Air Force Base
Dayton, Ohio
Attn: Dynamics Branch (1)
Aircraft Laboratory (1)
WCLSY (1)

Commanding Officer
USNNOEU
Kirtland Air Force Base
Albuquerque, New Mexico
Attn: Code 20 (Dr. J. N. Brennan) (1)

Chief, Bureau of Ships
Department of the Navy
Washington 25, D. C.
Attn: Code 106 (1)
Code 335 (1)
Code 345 (1)
Code 346 (1)
Code 420 (1)
Code 421 (1)
Code 423 (2)
Code 425 (1)
Code 440 (1)
Code 442 (2)
Code 443 (1)
Code 1500 (1)

Chief, Bureau of Naval Weapons
Department of the Navy
Washington 25, D. C.
Attn: RRMA (1)
RAAV-34 (1)
RAAD (1)
RAAD-2 (1)
RRSV-7 (1)
RRS-8 (1)
RSSH (1)
DLI-3 (1)
R (1)
RM (1)
RV (1)
RMLG (1)
RMGA (1)
RR (1)

Commanding Officer
Frankford Arsenal
Bridesburg Station
Philadelphia 37, Pennsylvania
Attn: Laboratory Division (1)

Special Projects Office
Bureau of Naval Weapons
Department of the Navy
Washington 25, D. C.
Attn: Missile Branch (2)
Technical Director (1)

Chief, Bureau of Yards and Docks
Department of the Navy
Washington 25, D. C.
Attn: Code D-202 (1)
Code D-202.3 (1)
Code D-220 (1)
Code D-222 (1)
Code D-410C (1)
Code D-440 (1)
Code D-500 (1)

Commanding Officer and Director
David Taylor Model Basin
Washington 7, D. C.
Attn: Code 140 (1)
Code 600 (1)
Code 700 (1)
Code 720 (1)
Code 725 (1)
Code 731 (1)
Code 740 (2)

Commander
U.S. Naval Ordnance Laboratory
White Oak, Maryland
Attn: Technical Library (2)
DE (1)
DR (1)
K (1)

Director
Materials Laboratory (1)
New York Naval Shipyard
Brooklyn 1, New York

Commander
Portsmouth Naval Shipyard (2)
Portsmouth, New Hampshire

Commander
Mare Island Naval Shipyard (2)
Vallejo, California

Commanding Officer and Director
U.S. Naval Electronics Laboratory (1)
San Diego 52, California

Officer-in-Charge
Naval Civil Engineering Research (2)
and Evaluation Laboratory
U.S. Naval Construction Battalion Center
Port Hueneme, California

Director
Naval Air Experiment Station
Naval Air Material Center
Naval Base
Philadelphia 12, Pennsylvania
Attn: Materials Laboratory (1)
Structures Laboratory (1)

Officer-in-Charge
Underwater Explosion Research Division (2)
Norfolk Naval Shipyard
Portsmouth, Virginia
Attn: Dr. H. M. Schauer

Commander
U.S. Naval Proving Ground (1)
Dahlgren, Virginia

Supervisor of Shipbuilding, USN and
Naval Inspector of Ordnance (1)
General Dynamics Corporation
Electric Boat Division
Groton, Connecticut

Supervisor of Shipbuilding, USN and
Naval Inspector of Ordnance (1)
Newport News Shipbuilding and Dry Dock Co.
Newport News, Virginia

Supervisor of Shipbuilding, USN and
Naval Inspector of Ordnance (1)
Ingalls Shipbuilding Corporation
Pascagoula, Mississippi

Commanding Officer
U.S. Naval Administrative Unit (1)
Massachusetts Institute of Technology
Cambridge 39, Massachusetts

Officer-in-Charge
Postgraduate School for Naval Officers (1)
Webb Institute of Naval Architecture
Crescent Beach Road
Glen Cove, Long Island, New York

Superintendent
Naval Weapons Plant (1)
Washington 25, D. C.

Commander
Naval Ordnance Test Station
China Lake, California
Attn: Physics Division (1)
Mechanics Division (1)

Commanding Officer
Naval Ordnance Test Station (1)
Underwater Ordnance Division
3202 E. Foothill Boulevard
Pasadena 8, California
Attn: Structures Division

Commanding Officer and Director
U.S. Naval Engineering Experiment Station
Annapolis, Maryland (1)

Superintendent
U.S. Naval Postgraduate School (1)
Monterey, California

Commandant
Marine Corps Schools
Quantico, Virginia
Attn: Director, Marine Corps Development Center (1)

Commanding General
U.S. Air Force
Washington 25, D. C.
Attn: Research and Development Division (1)

Commander
Air Material Command
Wright-Patterson Air Force Base
Dayton, Ohio
Attn: MCREX-B (1)
Structures Division (1)

Commander
U.S. Air Force Institute of Technology
Wright-Patterson Air Force Base
Dayton, Ohio
Attn: Chief, Applied Mechanics Group (1)

Director of Intelligence
Headquarters, U.S. Air Force
Washington 25, D. C.
Attn: P.V. Branch (Air Targets Division) (1)

Commander
Air Force Office of Scientific Research
Washington 25, D. C.
Attn: Mechanics Division (1)

U.S. Atomic Energy Commission
Washington 25, D. C.
Attn: Director of Research (2)

Director
National Bureau of Standards
Washington 25, D. C.
Attn: Division of Mechanics (1)
Engineering Mechanics Section (1)
Aircraft Structures (1)

Commandant
U.S. Coast Guard
1300 E. Street, N. W.
Washington 25, D. C. (1)
Attn: Chief, Testing and Development Division

U S. Maritime Administration
General Administration Office Building
441 G Street, N. W.
Washington 25, D. C
Attn: Chief, Division of Preliminary Design

National Aeronautics and Space Administration
1512 H Street, N. W.
Washington 25, D. C.
Attn: Loads and Structures Division (2)

Director
National Aeronautics and Space Administration
Langley Research Center
Langley Field, Virginia
Attn: Structures Division (2)

Director, Forest Products Laboratory
Madison, Wisconsin (1)

Federal Aviation Agency
Department of Commerce
Washington 25, D. C.
Attn: Chief, Aircraft Engineering Division (1)
Chief, Airframe and Equipment Branch (1)

National Sciences Foundation
1520 H Street, N. W.
Washington, D. C.
Attn: Engineering Sci. Div. (1)

National Academy of Sciences
2101 Constitution Avenue
Washington 25, D. C.
Attn: Technical Director, Committee on Ships' Structural Design (1)
Executive Secretary, Committee on Undersea Warfare (1)

General Dynamics Corporation
Electric Boat Division (1)
Groton, Connecticut

Ingalls Shipbuilding Corporation
Pascagoula, Mississippi (1)

Professor Lynn S. Beedle
Fritz Engineering Laboratory (1)
Lehigh University
Bethlehem, Pennsylvania

Professor R. L. Bisplinghoff
Department of Aeronautical Engineering (1)
Massachusetts Institute of Technology
Cambridge 39, Massachusetts

Professor H. H. Bleich
Department of Civil Engineering (1)
Columbia University
New York 27, New York

Professor B. A. Boley
Department of Civil Engineering (1)
Columbia University
New York 27, New York

Dr. John F. Brahtz
Department of Engineering (1)
University of California
Los Angeles, California

Dr. D. O. Brush
Structures Department 53-13 (1)
Lockheed Aircraft Corporation
Missile Systems Division
Sunnyvale, California

Professor B. Budiansky
Department of Mechanical Engineering (1)
School of Applied Sciences
Havard University
Cambridge 38, Massachusetts

Professor G. F. Carrier
Pierce Hall (1)
Havard University
Cambridge 38, Massachusetts

Professor Herbert Deresiewicz
Department of Civil Engineering (1)
Columbia University
632 W. 125th Street
New York 27, New York

Professor R. A. Di Taranto
Department of Mechanical Engineering (1)
Drexel Institute
32nd and Chestnuts Streets
Philadelphia, Pennsylvania

Professor D. C. Drucker, Chairman (1)
Division of Engineering
Brown University
Providence 12, Rhode Island

Professor A.C. Eringen
Department of Aeronautical Engineering (1)
Purdue University
Lafayette, Indiana

Professor J. Ericksen
Mechanical Engineering Department (1)
Johns Hopkins University
Baltimore 18, Maryland

Professor W. Fliigge
Department of Mechanical Engineering (1)
Stanford University
Stanford, California

Mr. Martin Goland, President
Southwest Research Institute (1)
8500 Culebra Road
San Antonio 6, Texas

Professor J. N. Goodier
Department of Mechanical Engineering (1)
Stanford University
Stanford, California

Professor L. E. Goodman
Engineering Experiment Station (1)
University of Minnesota
Minneapolis, Minnesota

Professor M. Hetenyi
The Technological Institute (1)
Northwestern University
Evanston, Illinois

Professor P. G. Hodge
Department of Mechanics (1)
Illinois Institute of Technology
Chicago 16, Illinois

Professor N. J. Hoff, Head
Division of Aeronautical Engineering (1)
Stanford University
Stanford, California

Professor Bruce G. Johnston
University of Michigan (1)
Ann Arbor, Michigan

Professor W. H. Hoppmann, II
Department of Mechanics (1)
Rensselaer Polytechnic Institute
Troy, New York

Professor J. Kempner
Department of Aeronautical Engineering and Applied Mechanics (1)
Polytechnic Institute of Brooklyn
333 Jay Street
Brooklyn 1, New York

Professor H. L. Langhaar (1)
Department of Theoretical and Applied Mechanics
University of Illinois
Urbana, Illinois

Professor B. J. Lazan, Director
Engineering Experiment Station (1)
University of Minnesota
Minneapolis 14, Minnesota

Professor E. H. Lee
Division of Applied Mathematics (1)
Brown University
Providence 12, Rhode Island

Mr. S. Levy
General Electric Research Laboratory (1)
3198 Chestnut Street
Philadelphia, Pennsylvania

Professor Paul Lieber
Geology Department (1)
University of California
Berkeley 4, California

Newport News Shipbuilding and Dry Dock Co.
Newport News, Virginia (1)

Professor Joseph Marin, Head
Department of Engineering Mechanics (1)
College of Engineering and Architecture
Pennsylvania State University
University Park, Pennsylvania

Professor R. D. Mindlin
Department of Civil Engineering (1)
Columbia University
632 W. 125th Street
New York 27, New York

Professor Paul M. Naghdi
Building T-7 (1)
College of Engineering
University of California
Berkeley 4, California

Professor William A. Nash (1)
Department of Engineering Mechanics
University of Florida
Gainesville, Florida

Professor N. M. Newmark, Head
Department of Civil Engineering (1)
University of Illinois
Urbana, Illinois

Professor E. Orowan
Department of Mechanical Engineering (1)
Massachusetts Institute of Technology
Cambridge 39, Massachusetts

Professor Aris Phillips
Department of Civil Engineering (1)
15 Prospect Street
Yale University
New Haven, Connecticut

Professor W. Prager, Chairman (1)
Physical Sciences Council
Brown University
Providence 12, Rhode Island

Professor J. R. M. Radok (1)
Department of Aeronautical Engineering and
Applied Mechanics
Polytechnic Institute of Brooklyn
333 Jay Street
Brooklyn 1, New York

Professor E. Reiss
Institute of Mathematical Sciences (1)
New York University
25 Waverly Place
New York 3, New York

Professor E. Reissner
Department of Mathematics (1)
Massachusetts Institute of Technology
Cambridge 39, Massachusetts

Professor M. A. Sadowsky (1)
Department of Mechanics
Rensselaer Polytechnic Institute
Troy, New York

Dr. Hyman Serbin
Design Integration Department (1)
Hughes Aircraft Company
Culver City, California

Professor Bernard W. Shaffer
Department of Mechanical Engineering (1)
New York University
University Heights
New York 53, New York

Professor J. Stallmeyer (1)
Department of Civil Engineering
University of Illinois
Urbana, Illinois

Professor Eli Sternberg (1)
Department of Mechanics
Brown University
Providence 12, Rhode Island

Dr. T. Y. Thomas (1)
Graduate Institute for Mathematics and Mechanics
Indiana University
Bloomington, Indiana

Professor S. P. Timoshenko
School of Engineering (1)
Stanford University
Stanford, California

Professor A. S. Velestos
Department of Civil Engineering (1)
University of Illinois
Urbana, Illinois

Dr. E. Wenk, Senior Specialist
Science and Technology (1)
Library of Congress
Washington 25, D. C.

Professor Dana Young
Yale University (1)
New Haven, Connecticut

Project Staff (10)

For your future distribution (10)